CHALMERS

Prediction of residual stresses in injection moulded parts

Master's Thesis in the Applied Mechanics

ANDREAS ÖSTERGREN

Department of Applied Mechanics
Division of Material and Computational Mechanics
CHALMERS UNIVERSITY OF TECHNOLOGY
Göteborg, Sweden 2013
Master's thesis 2013:02

MASTER'S THESIS IN APPLIED MECHANICS

Prediction of residual stresses in injection moulded parts

ANDREAS ÖSTERGREN

Department of Applied Mechanics
Division of Material and Computational Mechanics
CHALMERS UNIVERSITY OF TECHNOLOGY
Göteborg, Sweden 2013

Prediction of residual stresses in injection moulded parts
ANDREAS ÖSTERGREN

Master's Thesis 2013:02
ISSN 1652-8557
Department of Applied Mechanics
Division of Material and Computational Mechanics
Chalmers University of Technology
SE-412 96 Göteborg
Sweden
Telephone: + 46 (0)31-772 1000

Chalmers reproservice
Göteborg, Sweden 2013

Prediction of residual stresses in injection moulded parts
Master's Thesis in Applied Mechanics
ANDREAS ÖSTERGREN
Department of Applied Mechanics
Division of Material and Computational Mechanics
Chalmers University of Technology

ABSTRACT

For automotive plastic parts, mostly used for interior assemblies, there is a clear demand of an increased accuracy of the simulation model. One crucial input for the simulation model is the correct material data. Based on test data, it is known that the dynamic material properties of a plastic part can differ significantly from the material data given in the data sheet (which is based on a specimen). One assumption to explain the difference is the residual stresses caused by the injection moulding process.

A methodology has been developed to simulate the injection moulding process in Moldex3D and how the results can be used in other FEA structure analysis software. In this work, the focus has been to use the results from the injection moulding simulation in Abaqus within a parallel project.

To prepare for continuous analysis after the injection moulding simulation, a comparison between shell and solid elements was performed to evaluate the difference between the two models. In addition, since the number of elements through the thickness is important in injection moulding simulation, an investigation with 3, 5 and 7 elements through the thickness has been done.

The process parameters are crucial for the appearance and property for the final product. In order to determine how the process parameters influence the residual stress, only one parameter is changed at the time.

Keywords: Moldex3D, Injection moulding, Residual stress, Warpage, Abaqus

Contents

Preface

This Master thesis was carried out during autumn 2012 at Epsilon as the final part of the Master´s Programme in Applied Mechanics at Chalmers University of Technology.

First I would like to thank my supervisors, Jens Weber at Epsilon and Martin Fagerström at Chalmers, for the help and support. In addition, I would like to express my gratitude to Moldex3D support for lending a trial license to Moldex3D FEA Interface and patiently trying to answer all questions, especially, the theoretical questions for trying to explain the theoretical background of Moldex3D.

I would like to thank Maciej Wysocki for the valuable discussions and for the help with the polymer behaviour during injection moulding.

Finally, I would like to thank Hans Bjarnehed for the opportunity and for made this master thesis possible.

Göteborg June 2013

Andreas Östergren

Notations

Roman upper case letters

A	Area
A_1	Cross-WLF model parameter
$\tilde{A}_2$	Cross-WLF model parameter
$B(T)$	Pressure sensitivity
C	Constant in Modified Tait Model 2
C_{ijkl}	Elastic material stiffness
C_m	Specific heat of the mould
C_p	Heat capacity
D_1	Cross-WLF model parameter
D_2	Cross-WLF model parameter
E	Young's modulus
F	Force
Gr	Grashof number
H	Height
$\boldsymbol{I}$	Identity matrix
L_m	Characteristic length of the mould exterior surface
Nu	Nusselt number
P	Pressure
Pr	Prandtl number
Re	Reynolds number
$\dot{S}$	Rate of heat generation due to chemical reaction
T	Temperature
T_a	Air temperature
T_c	Coolant temperature
T_m	Mould temperature
T_s	Interface temperature between mould surface and air
T_t	Volumetric transition temperature
T_w	Interface temperature between mould and cooling channel
$\bar{T}$	Cycle-average mould temperature
V	Velocity

Roman lower case letters

b_{1L}	Model parameter in Modified Tait Model 2
b_{1S}	Model parameter in Modified Tait Model 2
b_{2L}	Model parameter in Modified Tait Model 2
b_{2S}	Model parameter in Modified Tait Model 2
b_{3L}	Model parameter in Modified Tait Model 2
b_{3S}	Model parameter in Modified Tait Model 2
b_{4L}	Model parameter in Modified Tait Model 2
b_{4S}	Model parameter in Modified Tait Model 2
b_5	Model parameter in Modified Tait Model 2
b_6	Model parameter in Modified Tait Model 2
b_7	Model parameter in Modified Tait Model 2
b_8	Model parameter in Modified Tait Model 2
b_9	Model parameter in Modified Tait Model 2

d_c	Diameter of cooling channel
f	Fractional volume function
g	Gravitational force
h_a	Heat transfer coefficient between mould and the ambient air
h_f	Heat transfer coefficient between mould and coolant
k	Thermal conductivity
k_a	Thermal conductivity of the ambient air
k_c	Thermal conductivity of the coolant
k_m	Thermal conductivity of the mould
n	Power-law index
p	Pressure
q	Heat flux
$\bar{q}$	Cycle-average heat flux
t	Time
t_T	Total cycle time
$\boldsymbol{u}$	Fluid velocity
u	Fluid velocity in x-direction
v	Fluid velocity in y-direction
w	Fluid velocity in z-direction

Greek letters

Γ	Boundary of the mould
Γ_p	Boundary of the mould, cavity surface
Γ_c	Boundary of the mould, cooling channel surface
Γ_e	Boundary of the mould, external surface
ΔT	Temperature difference
Φ	Source-term
α	Compressibility coefficient
α_{kl}	Coefficient of linear thermal expansion
β	Thermal expansion coefficient
$\dot{\gamma}$	Shear rate
ε_{ij}	Strain
ε_{ij}^0	Initial strain
η	Viscosity
η_0	Zero-shear rate viscosity
λ	Relaxation time
ν	Specific volume
ν_0	Specific volume at zero gauge pressure
ρ	Density
ρ_m	Mould density
σ	Stress
σ_{ij}^F	Initial stress
τ	Shear stress
τ^*	Relaxation stress
$\boldsymbol{\tau}$	Second-order deviatoric stress tensor

Abbreviations

ABS	Acrylonitrile-Butadiene-Styrene
CAE	Computer Aided Engineering
CFD	Computational Fluid Dynamics
CLTE	Coefficient of linear thermal expansion
EOC	End of cooling
EOF	End of filling
EOP	End of packing
FEA	Finite Element Analysis
FEM	Finite Element Method
GNF	Generalized Newtonian fluid
GTT	Group Trucks Technology
MAC	Modal Assurance Criterion
PVT	Pressure Volume Temperature
UCM	Upper Convected Maxwell
WLF	Williams, Landel, Ferry

1 Introduction

For automotive plastic parts, mostly used for interior assemblies, there is a clear demand of an increased accuracy of the simulation model. The reason for this demand is related to both a need to reduce the number of prototypes, in order to lower cost and save energy, and an increased number of load cases as e.g. Squeak & Rattle simulation.

One crucial input for the simulation model is the correct material data. Based on test data, it is known that the dynamic material properties of a plastic part can differ significantly from the material data given in the data sheet (which is based on a specimen). One assumption to explain the difference is the residual stresses caused by the injection moulding process.

1.1 Background

Volvo GTT has done some research for trying to understand what causes the difference in the dynamical response between a plastic part and the corresponding material data given in the data sheet.

The first test was a modal correlation test with 3D Laser Scanning. In this case, the evaluated structure was a shelf structure from Volvo GTT. The structure was mounted on a rigid frame and a shaker shook the structure, while a 3D laser scanner measured the structure, see Figure 1.1.

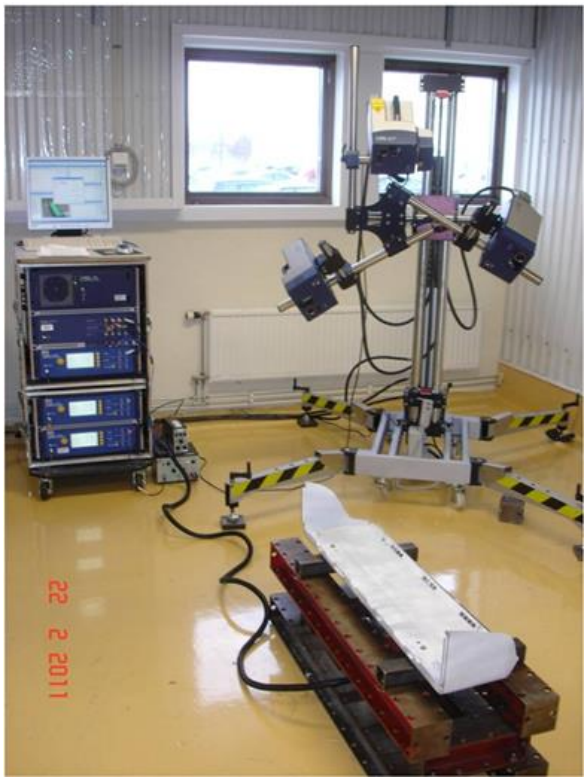

Figure 1.1 Test rig for shelf modal correlation.

After the physical test, a finite element method (FEM) simulation with the same setup was performed. In the first simulation, the Young's modulus of 2300 MPa was used, which is given in the data sheet. The results can be seen below in Table 1.1.

Table 1.1 Results from physical test and simulation for the shelf structured.

Mode #	Frequency Simulation [Hz] E = 2300 MPa	Frequency Test [Hz]	Frequency Simulation [Hz] E = 2900 MPa
1	24.0	26.1	26.9
2	26.6	29.6	29.8
3	31.1	35.0	35.0
4	39.4	45.4	45.1

Since the test setup gives very clear mode shapes, the correlation can be performed by just comparing the mode shapes between test and simulation visually. Therefore, the MAC value (Modal Assurance Criterion) definition is not necessary.

The results from the simulation with a Young's modulus of 2300 MPa gives lower frequencies than in the physical test. Since the mode shapes are independent of the Young's modulus (the part made of one isotropic material) the frequency can be tuned by changing the Young's modulus. By increasing the Young's modulus from 2300 MPa to 2900 MPa, the frequencies of all mode shapes are correlating much better. The same procedure was made with a front structure. The structure was mounted in the corners, according to Figure 1.2.

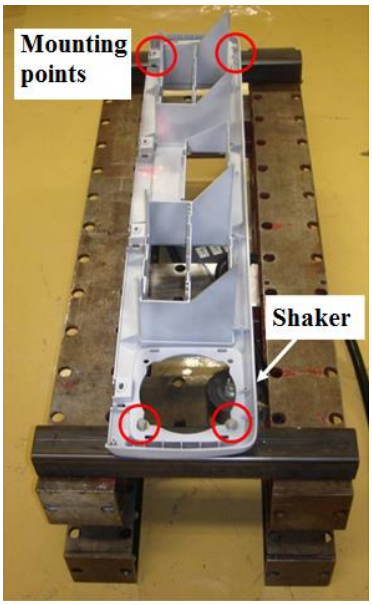

Figure 1.2 Location of mounting points for front structure.

The results from the simulation and the physical test are presented in the Table 1.2. As for the shelf structure, the Young's modulus had to be increased to get a good correlation. From these two experiments, front and shelf, there is obviously an increase of the Young's modulus with increasing complexity of the part.

Table 1.2 Results from simulation and physical test for the front structure.

Mode #	Frequency simulation [Hz] E = 2300 MPa	Frequency Test [Hz]	Frequency simulation [Hz] E = 3700 MPa
1	11.8	15.3	15.0
2	19.9	25.4	25.2
3	31.2	38.8	39.6
4	36.2	43.8	45.9
5	44.3	57.3	56.6
6	62.1	71.8	72.0
7	71.9	83.0	83.4

According to the simulations and physical tests, there is something that affects the change in Young's modulus, when defining it through a modal correlation and the corresponding data given in data sheet. After some further investigation, the conclusion was that this change probably is caused by the residual stresses from the manufacturing process.

1.2 Objective

The aim of the Master Thesis project has been to develop a methodology for simulating the injection moulding process in order to calculate the residual stresses, and how the results can be used in other FEA structure analysis software. For this type of simulation, all relevant process parameters have to be identified. The output (residual stress) will be utilised as input for a structural analysis, conducted within a parallel project, in order to study the effect on the modal behaviour.

1.3 Delimitations

The project is divided in two master thesis projects. This part of the project focuses on the injection moulding process, to determine the residual stresses by using the software Moldex3D. The other part of the project will focus on how the residual

stresses affects the modal analysis by using Abaqus. The front and shelf structures in section 1.1 are manufactured in Estonia. Due to lack of time and uncertainty to get the process parameter from Estonia, the front and shelf structure were not considered.

1.4 Method

In this work, the manufacturing simulation software Moldex3D is used to simulate the injection moulding process, HyperMold/Shell and HyperMold/Solid was used as pre-processor. The report starts with all relevant theory which has been used in this work. First, a comparison between shell and solid modelling was performed to evaluate the difference between the two elements types. The evaluated structure was a u profile structure, the geometry can be seen in Figure 1.3. The reason for this profile instead of a plate is to capture the 3D phenomena in the sharp corners. In this study, only the mesh and element type vary, all process parameters and material data are the same.

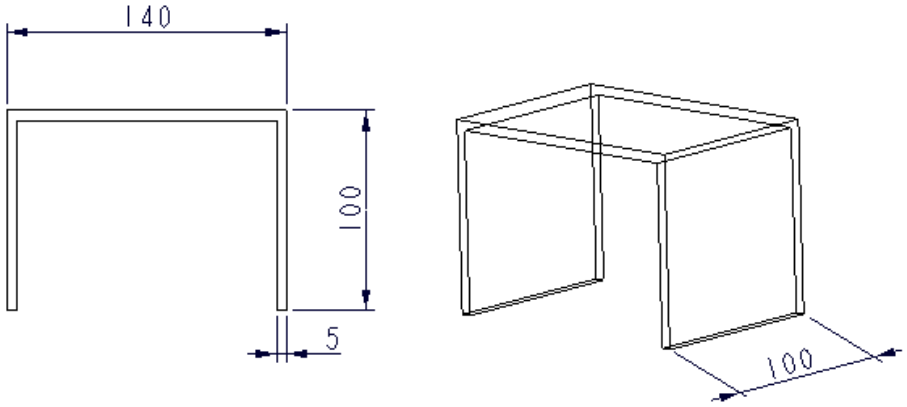

Figure 1.3 Geometry of the u profile structure in mm.

After the comparison between shell and solid element modelling, an investigation on number of elements through the thickness was performed. Since the number of elements through the part thickness is important for the injection moulding analysis.

Finally, the influence of process parameters on the resulting residual stress state and warpage is investigated. The investigated parameters are:

- Cooling
- Melt temperature
- Packing pressure
- Flow rate

The major output of this work is the residual stresses, which are then input for the second part of the project by using a mapping tool. After the mapping process, the residual stresses are used as load for a nonlinear warpage analysis in Abaqus where the stiffness matrix is updated. With this updated stiffness matrix a modal analysis is performed.

2 Introduction to injection moulding

Injection moulding is one of the most commonly used industrial processes to manufacture polymer parts. At high pressure, the molten plastic is injected into a mould, which is the inverse of the product's shape. Injection moulding can be used for a variety of parts, from the smallest component to larger products like outdoor furniture. Injection moulding is a cyclic process which means that it will return to the initial state after processing. An advantage of the process is that it can have a high production rate for parts with complex geometries. [1,2]

2.1 Injection moulding machine

One commonly used injection moulding machine is the screw injection moulding; a schematic machine is shown in Figure 2.1. Primarily it consists of two main components, an injection unit and a clamping unit. The injection unit consists of a hopper, a rotation screw, a heated barrel, a hydraulic or electric screw drive and a nozzle. The clamping unit contains the mould that is typically made of two halves.

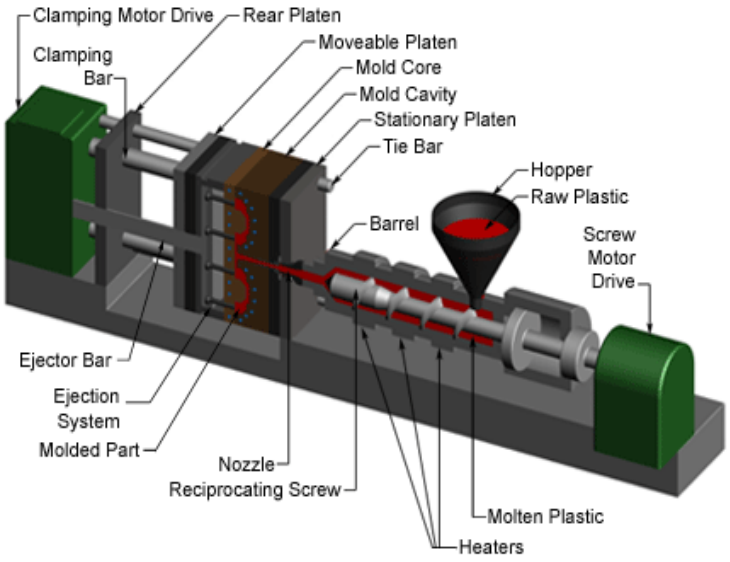

Figure 2.1 Schematic screw injection moulding machine, image from [3].

The hopper feed the machine with plastic granules. When the screw rotates, the granules move forward in the screw channel. The granules melts due to both conduction from heating units and friction heat generated by the rotating screw that force the granules against the wall. Finally, the injection moulding process cycle consists of the following four stages:

- Filling: the mould is closed and the screw moves forward and forces the melt into the mould cavity.
- Packing: to compensate for the volumetric shrinkage, more material is forced into the mould. By maintaining pressure, the surface characteristics get better

in the final product. This stage is also called the holding phase.

- Cooling: the cooling system plays an important role in injection moulding and the cooling time occupies 70-80% of the entire moulding cycle. Eventually, the gates have completely frozen and the cavity pressure is reduced to zero or a low value. The part continues to solidify as the heat is absorbed by the mould. A well-designed cooling system can shorten the cycle time, resulting in increased productivity and reduced cost .While cooling is taking place, the screw starts to move backwards to its initial position to accommodate the next charge of molten polymer.

- Ejection (demoulding): when the part has solidified and is stiff enough, the mould opens and the part is ejected. After ejection, the mould closes and the injection cycle starts again [1,2,4].

2.2 Feed system

When the polymer melt is injected from the nozzle it flows through the feeding system and finally enters the mould cavity. The feed system is a generic term for the sprue, runner and gate, an example of a feed system for a gearwheel is shown in Figure 2.2. It is important that the polymer in the runner does not solidify before the mould is completely filled. This can be accomplished in two ways, with an unheated (cold) runner using sufficiently large diameter in which the polymer solidifies *after* the polymer in the mould cavity, or with a heated (hot) runner in which the polymer does not solidify due to the high temperature. Moulding that are produced with a cold runner will eventually solidify, and the runner will be ejected with the part in each cycle. For the hot runner, insulation or heating will maintain the polymer at a melt temperature, and the runner will not be ejected with each cycle.

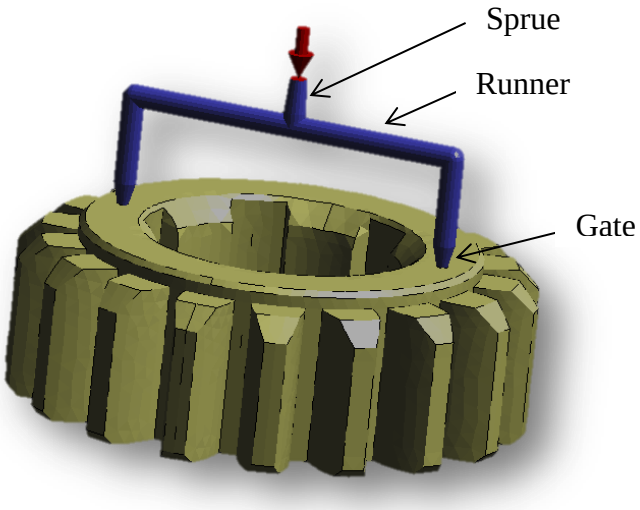

Figure 2.2 *An example of a feed system for a gearwheel, including the sprue, runner and gate.*

To ensure rapid and uniform filling, the location and dimension of the gate requires consideration. For symmetric and less complex parts it is easier to see were the gate should be located to get a uniform filling. But for more complex shapes, the location of the gate requires greater consideration. Producing larger parts often requires two or more gates. However, when the flow fronts from two gates meets, a weld line is created, which often is a weak point. To limit the weld line, the flow fronts must be fully molten. Furthermore, the position of the gates should be adjusted so that this weakness does not lie in an area where maximum mechanical strength is required [1,2,4].

3 Polymer materials

In order to understand the physical characteristic of polymer materials, an introduction to the molecular structure and thermal behaviour is presented. In addition, the polymer behaviour during injection moulding and the way it is modelled in Moldex3D are presented. The last part deals with the development of residual stress during and after injection moulding.

3.1 Molecular structure

Polymers (or macromolecules) consist of large numbers of molecular chains. Each chain is built up by the repetition of many small chemical units, called monomers, covalently bonded together, which are shown in Figure 3.1. A single mer is called a monomer, and comes from the Greek word *meros*, which means part. The term polymer was supposed to mean many parts [5,6].

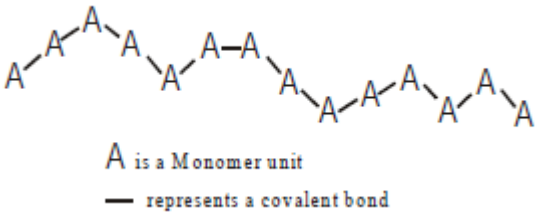

Figure 3.1 Schematic representation of a single polymer chain shows the monomer units and the covalent bond, image from [5].

The physical characteristics of a polymer depend on the molecular structure. Three possible molecular structures are represented schematically in Figure 3.2.

a) Linear polymer:

   Linear polymers consist of long single chains of monomers which are joined together end to end. In Figure 3.2a, a single linear polymer is represented, where each circle represents a monomer.

b) Branched polymer:

   The branched polymers have side-branch chains which are connected to the main chain, as can be seen in Figure 3.2b. The branches are considered to be part of the main chain molecule. The side branches reduce the chain packing efficiency which results in a lowering of the polymer density.

c) Cross-linked:

   The cross-linked polymers, which have a linear chain covalently bonded at various positions with another linear chain, as represented in Figure 3.2c. [5,6]

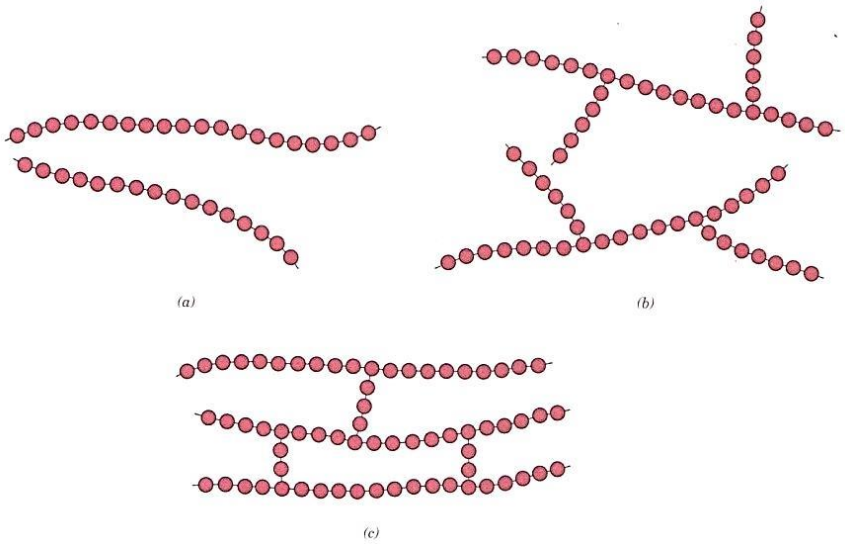

Figure 3.2 *Three types of molecular structures: (a) Linear (b) Branched and (c) Cross-linked, image from [6].*

The polymer behaviour does not only depend on the type of monomer and the molecular structure. It also depends on the arrangement of the polymer chains within a solid, known as the degree of crystallinity. The degree of crystallinity goes from completely amorphous to fully crystalline. In the amorphous polymer, the chains have a lack in order and are arrange in a random manner, while in fully crystalline polymer, the chains are organised in a repeating manner. The polymer chains are often only partially crystalline (or semicrystalline) since the polymer chains never are fully crystalline. Figure 3.3 shows a schematic representation of the amorphous polymer (a) and the semicrystalline polymer (b). [5,6]

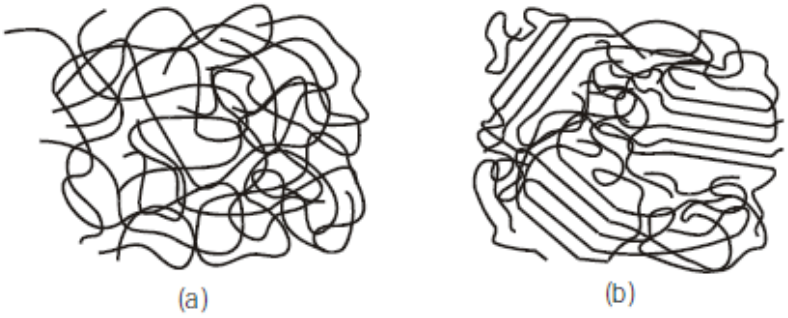

Figure 3.3 *(a) Amorphous polymer and (b) Semicrystalline polymer, image from [5].*

3.2 Thermal behaviour

Polymers are generally separated into thermoplastics and thermosets. Thermoplastics get soft and eventually melt upon heating. Therefore, a thermoplastic polymer can be used in the injection moulding process, since it can be reshaped. Thermoplastics usually consist of linear or branched chains, see Figure 3.2 ab, and are relatively soft and ductile. Thermoset polymers are generally harder, stronger and more brittle than thermoplastics, since they consist of cross-linked chains, see Figure 3.2c, but degrade upon heating and cannot be reshaped. [6]

3.3 ABS plastic

The material used in this work is the ABS plastic Terluran GP-22. Generally, ABS plastics are composed by three different monomers: acrylonitrile, butadiene, and styrene in varying proportions – the monomers can be seen in Figure 3.4. Each monomer adds special characteristics to the ultimate properties of the product:

- Acrylonitrile: chemical resistance, heat resistance and high strength
- Butadiene: toughness, impact strength and low-temperature property retention.
- Styrene: rigidity, surface appearance (gloss) and processability.

The ABS plastic is a copolymer, which means that two different monomers are linked in the same polymer chain, and it is made by polymerizing styrene and acrylonitrile in the presence of polybutadiene. [7,8]

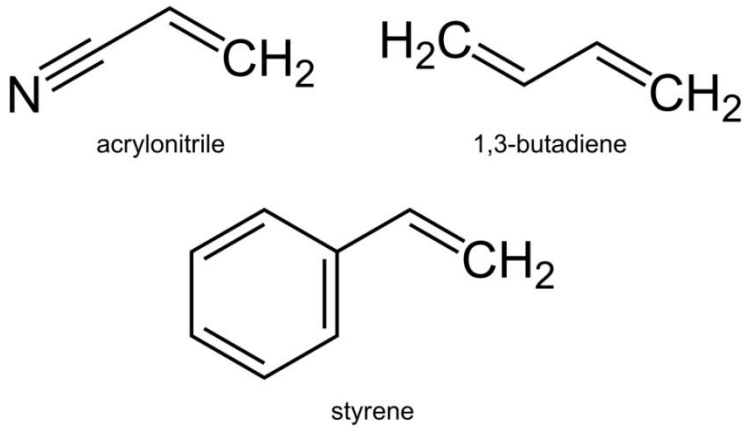

Figure 3.4 Monomers in ABS polymer, image from [8].

3.4 Polymer behaviour

To simulate the injection moulding process, it is important to represent the characteristics of the polymeric materials at different conditions. The following needs to be characterized; viscosity, viscoelasticity, Pressure-Volume-Temperature relationship (specific volume at different pressure and temperature), heat capacity and thermal conductivity. Each starts with a short introduction and followed by the way it is modelled in this work.

3.4.1 Viscous behaviour

Viscosity is a measure of a material's resistance to flow, and relates, in its simplest isotropic form, the shear stress to the shear strain rate. For e.g. water or oil, the viscosity is usually a constant value at constant temperature, which is generally referred to as Newtonian fluids. For thermoplastics, the viscosity is very complicated and varies nonlinearly, depending on the chemical structure, composition and processing conditions. For a given material, thermoplastics viscosity depends primarily on temperature, shear rate and pressure.

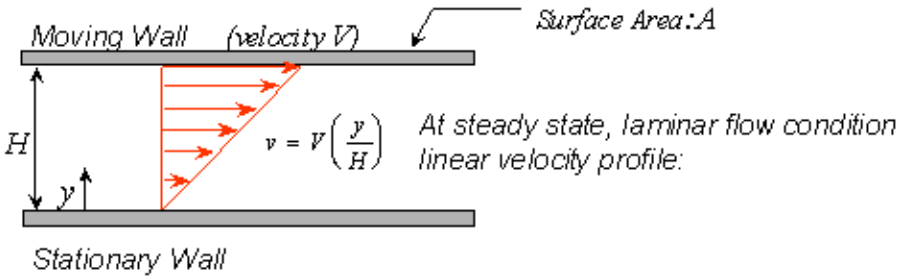

Figure 3.5 *Representation of the viscous flow that arise from shear stress imposed by two flat parallel plates, image from [9].*

The definition of a simple shear flow field is shown in Figure 3.5 for a Newtonian fluid. The upper wall is moving with constant velocity V and induces the flow of fluid between two parallel plates. At steady state, the velocity profile becomes linear. Therefore, the following can be defined according to Figure 3.5:

$$\tau = \frac{F}{A} \tag{3.1}$$

$$\dot{\gamma} = \frac{V}{H} \tag{3.2}$$

where τ is shear stress and $\dot{\gamma}$ is shear rate. From Equations (3.1) and (3.2), the viscosity can be defined as:

$$\eta = \frac{\tau}{\dot{\gamma}} \tag{3.3}$$

A higher viscosity, η, implies a higher resistance of flow to shear rate. Generally, for most thermoplastics, the viscosity curves have the same dependence on shear rates as shown in Figure 3.6.

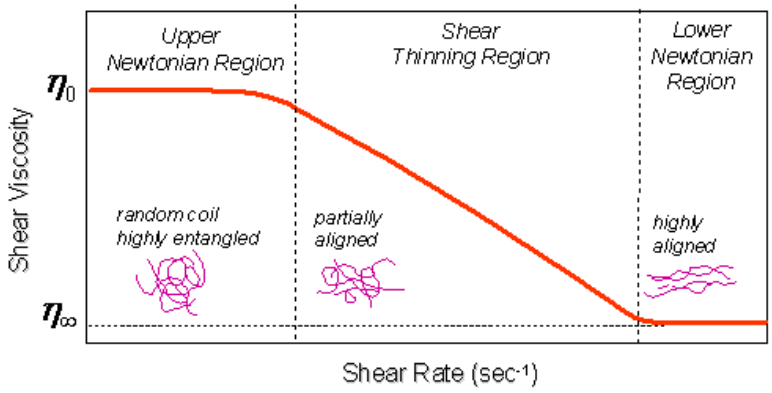

Figure 3.6 *Thermoplastics characteristic viscosity curve (log-log plot), image from [9].*

In the Upper Newtonian Region, located at lower shear rates, the viscosity is nearly constant. When the shear rate increases, the polymer chains are more uniformly aligned and the viscosity decreases accordingly. This region is called the Shear Thinning Region. In the Lower Newtonian Region, all polymeric chains are fully aligned and the shear viscosity becomes virtually insensitive to shear rate. [9]

3.4.2 Viscosity model in Moldex3D

There are some different mathematical models available to describe the viscosity in Moldex3D. The ABS plastic, Terluran GP-22, are used in all injection moulding simulations in this work. The recommended viscosity model for this material in Moldex3D is the Modified Cross Model 3, also known the Cross-WLF model. In this model, the melt viscosity, η, is a function of shear rate, $\dot{\gamma}$, temperature, T, and pressure, p, given by

$$\eta(\dot{\gamma}, T, p) = \frac{\eta_0(T,p)}{1 + \left(\frac{\eta_0(T,p)\dot{\gamma}}{\tau^*}\right)^{1-n}} \tag{3.4}$$

where η_0 is the zero-shear rate viscosity, n is the power-law index with a value between 0 and 1, τ^* is the relaxation stress. The zero-shear rate viscosity is based on the WLF (Williams, Landel and Ferry) functional form such that

$$\eta_0(T,p) = D_1 e^{\left(\frac{-A_1(T-T_c)}{A_2+(T-T_c)}\right)} \tag{3.5}$$

where T_c is given by:

$$T_c = D_2 + D_3 p \tag{3.6}$$

Finally, A_2 is given by

$$A_2 = \tilde{A}_2 + D_3 p \tag{3.7}$$

The model parameters $\left(n, \tau^*, D_1, D_2, D_3, A_1, \tilde{A}_2\right)$ are determined experimentally and are given in Moldex3D. For the material Terluran GP-22, the parameters in table 3.1 are available in Moldex3D.

Table 3.1 Cross-WLF model parameters for Terluran GP-22.

Symbol	Value
N	0.348
τ^*	24840 Pa
D_1	1.995×10^{17} $Pa\ sec$
D_2	343.15 K
D_3	0 K/Pa
A_1	40.455
$\tilde{A}_2$	51.6 K

The Cross-WLF model with the material Terluran GP-22 gives the viscosity versus shear rate as shown in Figure 3.7 for the temperatures 220 C°, 250 C° and 280 C° respectively. [9]

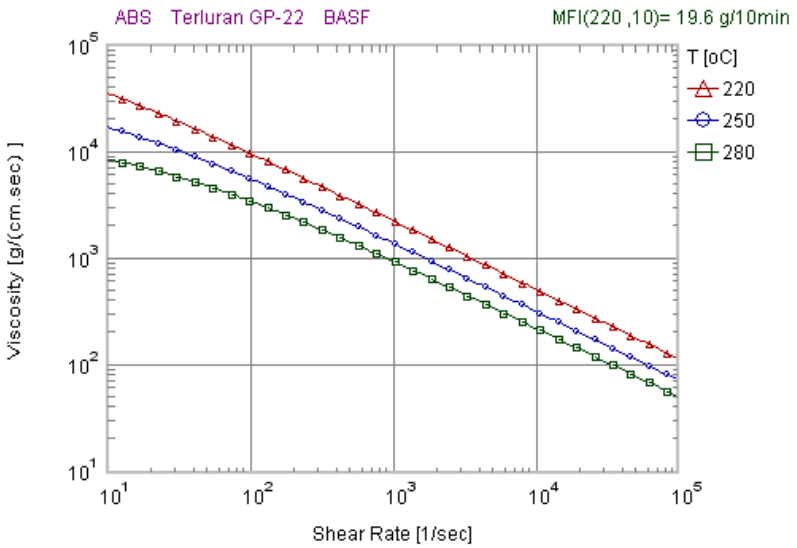

Figure 3.7 *Viscosity versus shear rate for Terluran GP-22 for the temperatures 220 C°, 250 C° and 280 C° respectively.*

3.4.3 Viscoelasticity

At low temperature, an amorphous polymer may behave like a glass. And for relative small deformations, the mechanical behaviour may be elastic. At high temperatures, the polymer melt behaves like a viscous liquid. For intermediate temperatures (above the glass transition temperature), polymer behaves like a rubbery solid that exhibit a combination of elastic and viscous behaviour; the conditions is denoted viscoelasticity.

In the instant when stress is applied or released, deformation of the elastic body occurs, *i.e.* the strain is independent of time. In addition, after the stress is released, the deformation is totally recovered, which means that it returns to its original shape. This behaviour is visualized in Figure 3.8b as strain versus time for the load time curve shown in Figure 3.8a, where load is applied at time t_a and released at t_r.

The totally viscous behaviour is not instantaneous, which means that deformation is delayed and dependent on the *rate* of the applied stress. In addition, upon release of stress, the deformation is not reversible or completely recovered. This behaviour is represented in Figure 3.8d.

The viscoelastic behaviour is illustrated in Figure 3.8c, the load versus time in Figure 3.8a results in an instantaneous elastic strain, which is followed by a viscous, time-dependent strain. [6]

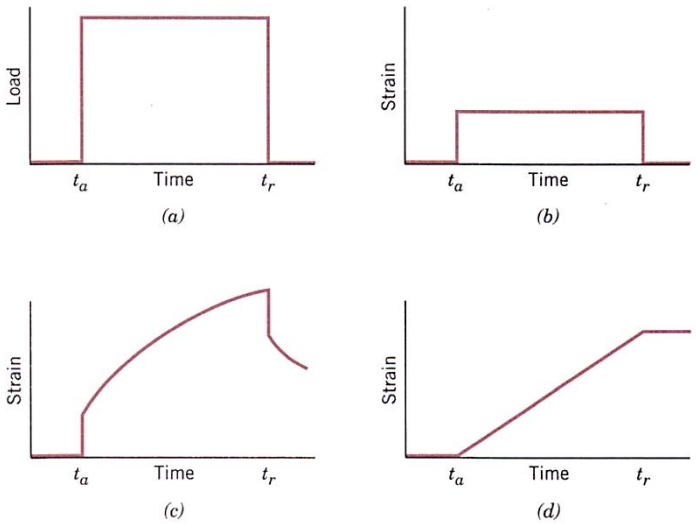

Figure 3.8 *For the load versus time cycle in (a), the strain versus time response is totally elastic (b), viscoelastic, and viscous (d) behaviour, image from [6].*

Material rheology of viscoelasticity is mainly defined by two parts, viscosity and relaxation time. Viscosity is introduced in section 3.4.1 and relaxation time λ is defined as the time required for stress to be reduced to half of its original value. For typical thermoplastics, the relaxation time is a function of the plastics composition, temperature, pressure, shear rate, etc. Similar to the viscosity, the relaxation time of thermoplastics generally decreases when temperature and shear rate increase. [9]

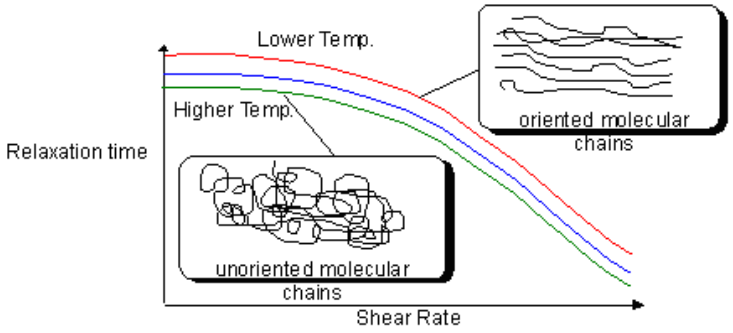

Figure 3.9 *Relaxation time of plastic molecules in processing, image from [9].*

3.4.4 Viscoelasticity model in Moldex3D

In the viscosity model described in section 3.4.2, the polymer melt is modeled as a Generalized Newtonian fluid (GNF) using the cross model to describe viscosity, which generally can predict a satisfying pressure and velocity. However, to provide more precise results, especially for predicting residual stress and molecular orientation, the viscoelastic nature of the polymer needs to be accounted for. In Moldex3D there are some different kinds of mathematical models available for viscoelasticity. The model used in this work is the White-Metzner Model which is modified from the Upper Convected Maxwell Model (UCM). The UCM model can be

represented by a viscous damper and an elastic spring connected in series according to Figure 3.10

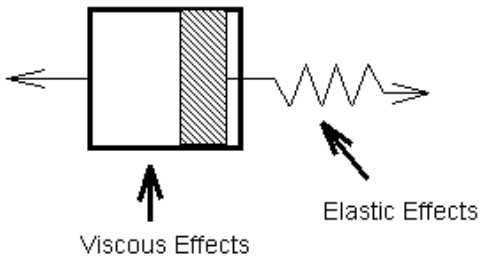

Figure 3.10 A viscous damper and an elastic spring represent the model.

Both models use the following relation between stress, stress rate and strain rate.

$$\tau + \lambda(T,\dot{\gamma})\left(\frac{\partial \tau}{\partial t} + \boldsymbol{u}\cdot\nabla\tau - \nabla\boldsymbol{u}^T\cdot\tau - \tau\cdot\nabla\boldsymbol{u}\right) = \eta(T,\dot{\gamma})(\nabla\boldsymbol{u} + \nabla\boldsymbol{u}^T) \qquad (3.8)$$

where τ is the stress, $\boldsymbol{u}$ is the fluid velocity and λ is the relaxation time. The relaxation time and viscosity, η, are both function of temperature and shear rate. The difference between the two models is how the relaxation time is defined. In the White-Metzner Model, the relaxation time is defined as

$$\lambda(T,\dot{\gamma}) = \frac{\eta(T,\dot{\gamma})}{G} \qquad (3.9)$$

The modulus G is given in Moldex3D for the material Terluran GP-22 and the value $G = 180000$ Pa is used in this work. [9]

3.4.5 Pressure-Volume-Temperature relationship

Another crucial characteristic of injection moulding is the PVT (Pressure-Volume-Temperature) relationship, since thermoplastic generally undergoes a significant volumetric change over temperature and pressure. The PVT diagram shows the compressibility of polymers which is a result from melt temperature and applied pressure.

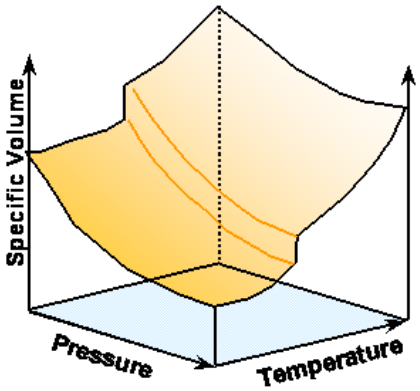

Figure 3.11 Schematic representation of the specific volume dependence on pressure and temperature, image from [9].

The specific volume (inversely proportional to density) of thermoplastics varies during the phase changes. For a specific material, the specific volume change depends on the temperature and pressure of the processes, which is represented schematically in Figure 3.11.

Depending on the degree of crystallinity, the specific volume behaves differently in the transition near the melting point from solid state to liquid state. The specific volume for crystalline thermoplastics exhibits a prominent transition near the melting point, the amorphous thermoplastics have a gradual transition for such phase change, as can be seen below in Figure 3.12.

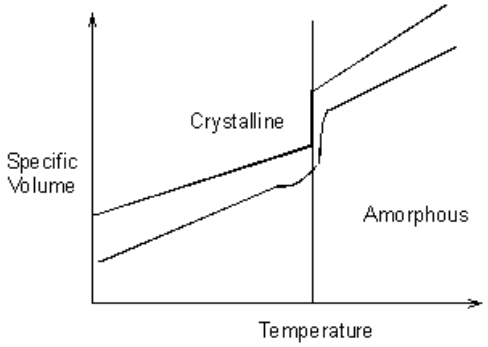

Figure 3.12 Crystalline and amorphous thermoplastics behaviour during phase changes, image from [9].

3.4.6 PVT model in Moldex3D

The PVT relationship can be described with the Modified Tait Model 2, which is used in this work, and is given by

$$v(T,p) = v_0(T)\left[1 - Cln\left(1 + \frac{p}{B(T)}\right)\right] + v_t(T,p) \tag{3.10}$$

where $v(T,p)$ is the specific volume (inversely proportional to density) at temperature, T, and pressure, P, $v_0(T)$ is the specific volume at zero gauge pressure, C is a constant of 0.0894, and $B(T)$ accounts for the pressure sensitivity of the material. For the upper temperature region ($T > T_t$) and the lower temperature region ($T \leq T_t$) respectively, the following relations are used.

$$v_0(T) = \begin{cases} b_{1S} + b_{2S}\bar{T}, & if\ T \leq T_t \quad (3.11a) \\ b_{1L} + b_{2L}\bar{T}, & if\ T > T_t \quad (3.11b) \end{cases}$$

$$B(T) = \begin{cases} b_{3S}e^{-b_{4S}\bar{T}}, & if\ T \leq T_t \quad (3.12a) \\ b_{3L}e^{-b_{4L}\bar{T}}, & if\ T > T_t \quad (3.12b) \end{cases}$$

$$v_t(T,p) = \begin{cases} b_7 e^{(b_8\bar{T} - b_9 p)}, & if\ T \leq T_t \quad (3.13a) \\ 0\,, & if\ T > T_t \quad (3.13b) \end{cases}$$

where $\bar{T}$ is defined by

$$\bar{T} = T - b_5 \tag{3.14}$$

Finally, the volumetric transition temperature, T_t, depends on pressure and can be described by

$$T_t = b_5 + b_6 p \tag{3.15}$$

The model parameters $(b_{1L}, b_{1S}, b_{2L}, b_{2S}, b_{3L}, b_{3S}, b_{4L}, b_{4S}, b_5, b_6, b_7, b_8, b_9)$ are material parameters, obtained by fitting PVT data [10]. In Moldex3D, the model parameters are given and are shown in Table 3.2 for the material Terluran GP-22.

Table 3.2 Modified Tait Model 2 parameters for Terluran GP-22.

Symbol	Value
b_{1L}	$0.0009896\ m^3/Kg$
b_{2L}	$6.13 \times 10^{-7}\ m^3/(Kg.K)$
b_{3L}	$1.87878 \times 10^8\ Pa$
b_{4L}	$0.00462\ 1/K$
b_{1S}	$0.0009896\ m^3/Kg$
b_{2S}	$3.411 \times 10^{-7}\ m^3/(Kg.K)$
b_{3S}	$2.19437 \times 10^8\ Pa$
b_{4S}	$0.005151\ 1/K$
b_5	$383.15\ K$
b_6	$1.38 \times 10^{-7}\ K/Pa$
b_7	$0\ m^3/Kg$
b_8	$0\ 1/K$
b_9	$0\ 1/Pa$

The specific volume dependence on temperature and pressure for Terluran GP-22, when the Modified Tait Model 2 is utilised, shown in Figure 3.13. [9]

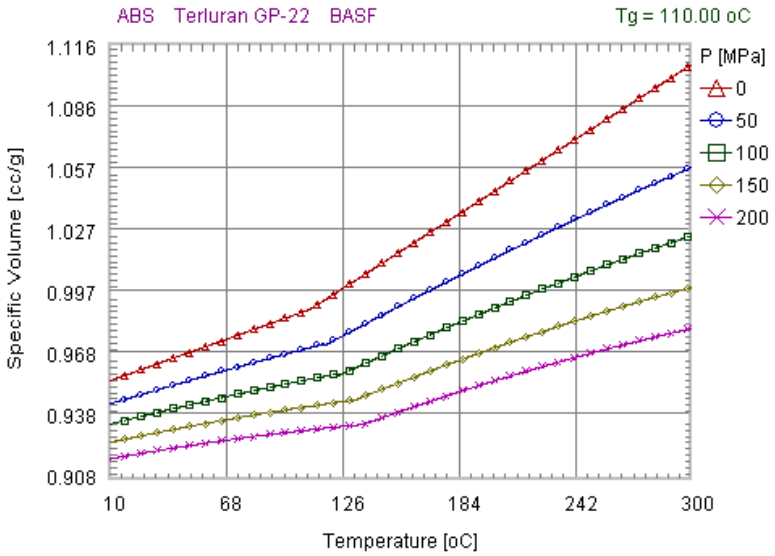

Figure 3.13 PVT diagram for Terluran GP-22.

3.4.7 Heat capacity

The heat capacity is defined as the amount of thermal energy required to increase the temperature one degree per unit mass of the polymer. Thus, polymers which are less sensitive to temperature variation have a higher heat capacity.

In this work, the heat capacity is assumed to be a constant value. For the material, Terluran GP-22, the heat capacity is $C_p = 2300\, J/(Kg.K)$. [9]

3.4.8 Thermal conductivity

Thermal conductivity is the material's ability to conduct heat. The ability of thermal conduction for heat transmittance increase with higher thermal conductivity. Typically, the thermal conductivity a polymer will increase with increased temperature, especially for crystalline polymers. Amorphous thermoplastics have a smooth relation between thermal conductivity and temperature variation.

Thermal conductivity does not vary significantly from one thermoplastic to the other and is relatively insensitive to temperature and independent of molecular weight. Generally, the thermal conductivity of thermoplastics is relative low as compared to the mould metal. The heat transferred to the surroundings is reduced with low thermal conductivity. For high viscosity thermoplastics, considering the heat dissipated by viscous forces, the temperature distribution through the thickness is therefor quite non-isothermal.

In this work, the thermal conductivity is assumed to be independent of temperature and is constant. For the material Terluran GP-22, the thermal conductivity is $k = 0.16\, W/(m.K)$. [9]

3.5 Residual stress

Residual stresses are the stresses remaining inside the moulded product under the condition of no external loads. Internal stresses are frozen inside the part in the moulding process. Residual stresses affect a part similarly to externally applied stresses and are the main cause of part shrinkage and warpage. There are two types of residual stress, flow-induced residual stress and thermal-induced residual stress. [11]

3.5.1 Flow-induced residual stress

When the temperature is higher than the melt temperature, *i.e*. in a molten state, the long polymer chain molecules are unstressed and tend to conform to a random-coil state of equilibrium. The orientation of the molecules during processing is directed along the flow, as the polymer is sheared and elongated. When the part solidifies, the molecular orientation is locked within the moulded part. If the moulded part solidifies before the polymer molecules are fully relaxed to their state of equilibrium, this result in frozen-in stress, often referred to as flow-induced residual stress.

There is a highly oriented frozen layer at the part surface, see Figure 3.14, due to a combination of high shear stress and a high cooling rate adjacent to the mould wall. The highly oriented frozen-in molecules typically results in part warpage. The polymer melt in the hot core is able to relax to a higher degree, due to the thermal insulating effect of the frozen layers, leading to a low molecular orientation zone. [11]

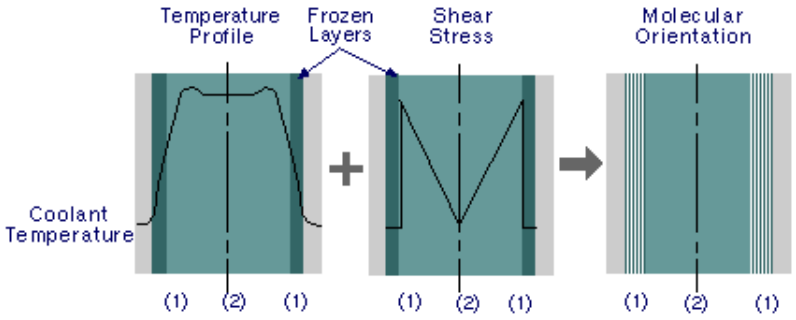

Figure 3.14 *Development of flow-induced residual stresses due to highly oriented frozen-in molecular. Darker area represent frozen layers and (1) high cooling, shear, and orientation zone (2) Low cooling, shear, and orientation zone, image from [11].*

3.5.2 Thermal-induced residual stress

The thermal-induced residual stresses occur due to several reasons. One of them is uneven material shrinkage during injection moulding. It can be demonstrated with a free quenching example, in which a part of uniform temperature is suddenly sandwiched by cold mould walls. In the beginning of the cooling stages, when the external surface layers cool down and start to shrink, the core is still molten and free to contract. However, the rigid external layers constrain thermal contraction when the internal core cools. This results in thermal-induced residual stresses. The stress distribution through the thickness can be seen in Figure 3.15, where tensile stresses appear in the core, balanced by compression in the outer layers, which generally enhance fatigue properties. [11]

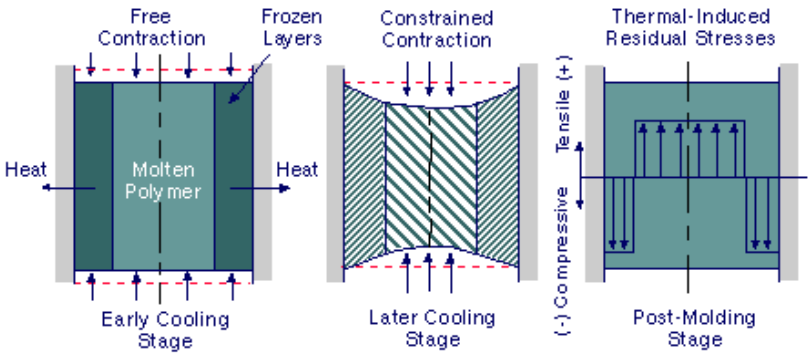

Figure 3.15 *Thermal-induced residual stress caused by uneven material shrinkage, image from [11].*

Another reason for the thermal-induced residual stresses is unbalanced cooling; a variation in the cooling rate from the mould wall to its center. If the cooling rate of the two outer surfaces is unbalanced, asymmetrical thermal-induced residual stresses can occur. This results in an asymmetric tension-compression pattern across the part and gives rise to a bending moment that will cause part warpage, which can be seen in Figure 3.16. Parts with non-uniform thickness or poorly cooled areas are also prone to unbalanced cooling, and thus to thermally-induced residual stresses. [11]

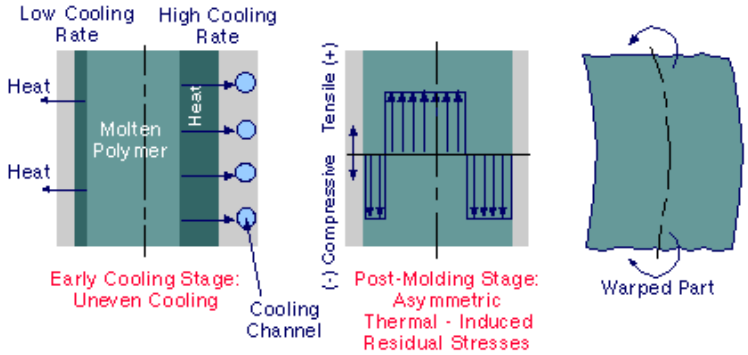

Figure 3.16 *Thermal-induced residual stress caused by unbalanced cooling, image from [11].*

One more reason for the thermal-induced residual stresses is differential shrinkage. The temperature profile through the part thickness is shown in Figure 3.17a. The cross section is divided in eight equal layers for the purpose of illustration and the temperatures are at solidification for each layer. A typical pressure history is shown in Figure 3.17b, the pressure levels p1 to p8 corresponds to the temperature layers t1 to t8. From the pvt plot, Figure 3.17c, the final frozen-in specific volume for each layer can be determined, marked by a solid circle. [11]

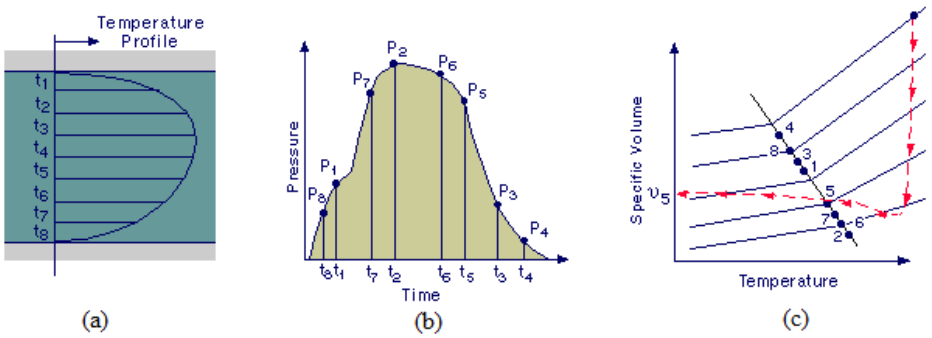

Figure 3.17 Development different frozen-in specific volume through the part thickness, image from [11].

The part deforms as layers of different frozen-in specific volume interact with each other. Figure 3.18 shows a schematically representation of differential shrinkage. If the layer were detached from each other, the layers in Figure 3.18a would shrunk like those in Figure 3.18b. In reality, the layers are bound together and therefore the shrinkage distribution appears as in Figure 3.18c, resulting in thermally-induced residual stresses. [11]

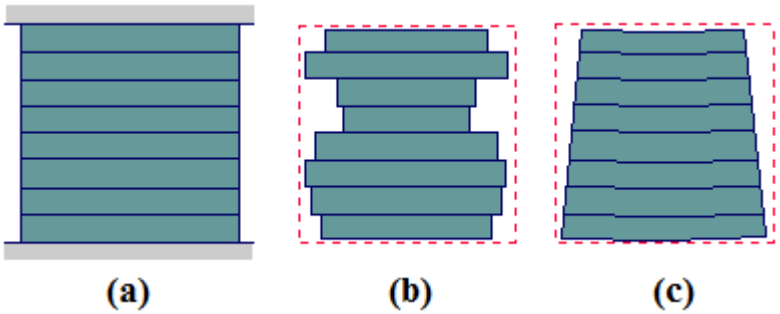

Figure 3.18 Schematically representation of differential shrinkage, image from [11].

4 Injection moulding simulation

To simulate the injection moulding process, Moldex3D R11 is used, which is a comprehensive CAE tool for injection moulding. In Moldex3D there are some different modules available to simulate the injection moulding process, which are; flow, packing and cooling analysis, all described below. Moldex3D use CFD (Computational Fluid Dynamics) analysis in order to simulate the filling and packing stage. Further, Moldex3D also support warpage analysis for both shell and solid modelling, which follows the same procedure, therefore only the warpage analysis for the shell model is described.

The majority of the plastic products have a thin shell structure, *i.e.*, their thickness is small compared to other dimensions. In these cases, it may be a good approximation to use the shell model.

4.1 Shell model in Moldex3D

The Shell model applies conservation of mass, conservation of momentum and conservation of energy, described below, to simulate injection moulding process. The thin solid parts are simplified to a 2.5D midplane model with assigned thickness, according to Figure 4.1. The 2D midplane can vary in thickness, therefore 2.5D.

4.1.1 Flow and packing analysis

The injection moulding process is theoretically a three-dimensional, transient problem with moving melt front. The mathematical models for Shell-Flow in Moldex3D are governed by conservation of mass, conservation of momentum and conservation of energy under non-isothemal and compressible condition. The Shell-Flow flow also omits the calculation of the velocity component and the thermal convection in the thickness direction.

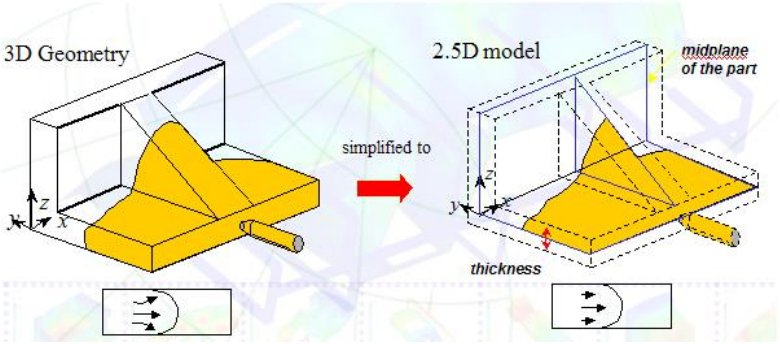

Figure 4.1 *Thin solid geometry is simplified to a mid-plane model, image from [9].*

Let x and y denote the planar coordinates and z the thickness direction coordinate. Furthermore, the velocity components u, v and w are in the x, y and z direction respectively. Conservation of mass, states that mass neither can be created nor destroyed, so the change in mass must only change due to flux through the surface bounding a fix control volume. Consequently, the mass conservation or continuity

equation is given (on spatial form) with the velocity component in thickness direction, w, neglected.

$$\frac{\partial \rho(T,p)}{\partial t} + \frac{\partial}{\partial x}(\rho(T,p)u) + \frac{\partial}{\partial y}(\rho(T,p)v) = 0 \tag{4.1}$$

The law of conservation of momentum, states that, within a certain control volume, the total momentum remains constant, whereby.

$$\rho \frac{D\boldsymbol{u}}{Dt} = -\nabla p + \nabla \cdot \boldsymbol{\tau} + \rho \boldsymbol{g} \tag{4.2}$$

were p is the pressure, $\boldsymbol{\tau}$ is the deviatoric stress tensor, $\boldsymbol{g}$ is the gravitational force and $\frac{D\boldsymbol{u}}{Dt}$ is the material derivative of the velocity field. Under steady state conditions in the absence of gravity effect, Equation 4.2 can be reduced to.

$$\nabla \cdot \boldsymbol{\tau} = \nabla p \tag{4.3}$$

Which for a viscous fluid takes the following component form.

$$\mathrm{x-component} \qquad -\frac{\partial p}{\partial x} + \frac{\partial}{\partial z}\left(\eta(\dot{\gamma},T,p)\frac{\partial u}{\partial z}\right) = 0 \tag{4.4}$$

$$\mathrm{y-component} \qquad -\frac{\partial p}{\partial y} + \frac{\partial}{\partial z}\left(\eta(\dot{\gamma},T,p)\frac{\partial v}{\partial z}\right) = 0 \tag{4.5}$$

The law of conservation of energy, states that energy can be changed from one form to another but cannot be created or destroyed. It is convenient to express this relation in terms of the fluid temperature, T, and the specific heat, C_p. Therefore, it could be expressed as

$$\rho C_p\left(\frac{\partial T}{\partial t} + \boldsymbol{u} \cdot \nabla T\right) = \nabla(\boldsymbol{k}\nabla T) + \Phi \tag{4.6}$$

where k is the thermal conductivity and Φ is a source-term. The source-term is defined as, $\Phi = \eta\dot{\gamma}^2 + \Delta\dot{H} + \ldots$,the first term $\eta\dot{\gamma}^2$ is viscous dissipation effect, and the rest include reaction term and other effects. In Moldex3D/Shell, only the viscous dissipation effect is considered. According to the earlier assumptions, Equation 4.6 can be reduced as

$$\rho C_p\left(\frac{\partial T}{\partial t} + u\frac{\partial T}{\partial x} + v\frac{\partial T}{\partial y}\right) = k\frac{\partial^2 T}{\partial z^2} + \eta\dot{\gamma}^2 \tag{4.7}$$

The above procedures simplified the conservation of mass (Equation 4.1), momentum (Equation 4.5), and energy (Equation 4.7) these equations together with the viscosity model in section 3.4.3 and pvT model in section 3.4.6, are the governing equations to simulate the flow in a thin cavity. [9,12,13]

4.1.2 Cool analysis for shell model

The basic procedure for the cooling in the injection moulding process is that the heat is transferred from the polymer to the cooling channels by heat conduction, and the heat is then removed with the coolant by heat convection. After the part has been ejected, it continues to cool down to room temperature by dissipating the thermal energy into air. Figure 4.2 shows schematically the cooling in injection moulding.

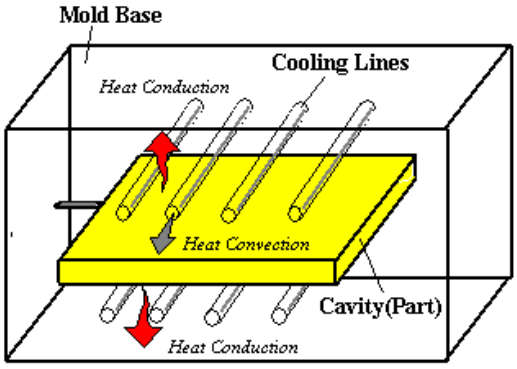

Figure 4.2 *Schematically representation of the cooling in injection moulding, image from [9].*

In reality, the mould temperature varies during the cycle, and when it is controlled properly, the temperature variation is repeated in each cycle. Figure 4.3 shows a typical mould temperature variation. In this case, the mould temperature variation is assumed to an average mould temperature.

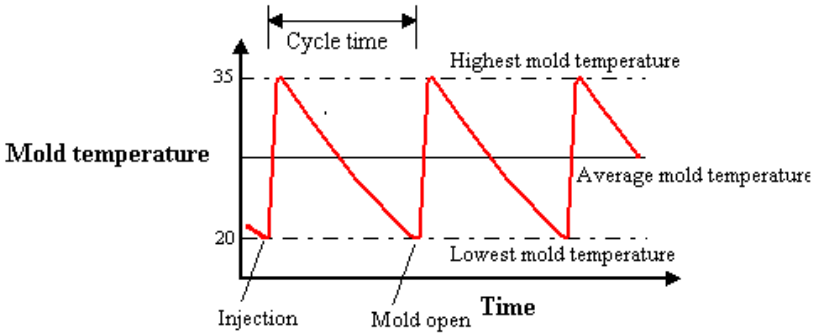

Figure 4.3 *The mould temperature variation in each cycle is periodic, image from [9].*

The governing equation for the cooling stage is the steady-state Laplace equation to model the thermal behaviour.

$$k_m\left(\frac{\partial^2\bar{T}}{\partial x^2}+\frac{\partial^2\bar{T}}{\partial y^2}+\frac{\partial^2\bar{T}}{\partial z^2}\right)=0 \tag{4.8}$$

where $\bar{T}$ is the cycle-average mould temperature and k_m is the mould thermal conductivity. By solving the equation; a cycle-Averaged temperature distribution can be obtained.

The boundary of the mould, Γ, includes the cavity surface, Γ_p, the cooling channel surface, Γ_c, and the external surface, Γ_e. The boundary conditions are as follows:

- Mould cavity surface

$$k_m\frac{\partial T}{\partial n}=-\bar{q},\quad in\ \Gamma_p \tag{4.9}$$

where $\bar{q}$ is the cycle-averaged heat flux across the melt and mould interface, according to

$$\bar{q} = \frac{1}{t_T}\int_0^{t_T} q(t)dt \tag{4.10}$$

where t_T is the total cycle time.

- Cooling channel surface

$$k_m \frac{\partial T}{\partial n} = -h_f(T_w - T_c), \quad in\ \Gamma_c \tag{4.11}$$

where h_f is the heat transfer coefficient between the mould and the coolant, T_w is the interface temperature between mouldbase and cooling channels, and T_c is the coolant temperature. The heat transfer coefficient h_f is given by [1]

$$h_f = \frac{Nu \cdot k_c}{d_c} \tag{4.12}$$

where d_c is the diameter of the cooling channel, k_c is the thermal conductivity of the coolant, and Nu is the Nusselt number. The recommended empirical Nusselt number according to Dittus and Boelter [14] are

$$Nu = 0.023 Re^{4/5} Pr^{0.4} \tag{4.13}$$

where Re is Reynolds number and Pr is Prandtl number.

- Mould exterior surface

$$k_m \frac{\partial T}{\partial n} = -h_a(T_s - T_a), \quad in\ \Gamma_e \tag{4.14}$$

where T_s is the interface temperature between mould surface and air, T_a is the temperature of the ambient air and h_a is the heat transfer coefficient between the mould and the ambient air, and is given by

$$h_a = \frac{k_a \overline{Nu}}{L_m} \tag{4.15}$$

where k_a is the thermal conductivity of the ambient air, L_m is the characteristic length of the mould exterior surface, and $\overline{Nu}$ is the Nusselt number, for a variety of circumstances, the Nusselt number can be expressed by

$$\overline{Nu} = C(Gr\ Pr)^m \tag{4.16}$$

where Gr is the Grashof number and Pr is the Prandtl number of air. The values of C and m depends on the particular case; for example, $C = 0.1$ and $m = 1/3$ for vertical planes, $C = 0.54$ and $m = 1/4$ for free convection from upper horizontal planes, and $C = 0.58$ and $m = 1/5$ for free convection from bottom horizontal planes [15]

There are two different ways to analyse the cooling channel system, normal cooling channel analysis and cooling channel network analysis. In this work, the normal cooling channel analysis is used and it assumes that the rise of coolant temperature is neglected, which results in that the coolant temperature in Equation 4.11 is considered as a constant value during the cycle. [1,9]

4.1.3 Warp analysis for shell model

The assumptions made in the warpage analysis are that the materials of the parts are linear elastic, the strains are small and the deformation of the structure is quasi-static. The governing equations to solve the displacement problem are the following equilibrium equation.

$$\nabla \boldsymbol{\sigma} + \boldsymbol{F} = 0 \tag{4.17}$$

where $\boldsymbol{\sigma}$ represent the stress and **F** is the body force and the thermal load. When the part is fully constrained in the mould, no calculation of displacement is required. After the part is ejected the strain components may be non-zero, and following elastic stress-strain relation can be used.

$$\sigma_{ij} = C_{ijkl}(\varepsilon_{kl} - \varepsilon_{kl}^{0} - \alpha_{kl}\Delta T) + \sigma_{ij}^{F} \tag{4.18}$$

where σ_{ij} is the stress component, σ_{ij}^{F} is the initial stress, *i.e.*, the flow- and thermally induced residual stress, ε_{ij} infinitesimal elastic strain component, ε_{ij}^{0} initial strain from pvT effects, C_{ijkl} elastic material stiffness, α_{kl} coefficient of linear thermal expansion and ΔT temperature difference. Furthermore, the elastic strain components are (as usual) defined by.

$$\varepsilon_{ij} = \frac{1}{2}\left(u_{i,j} + u_{j,i}\right) \tag{4.19}$$

In addition, the analysis approach of in-mould constrains effect combines part and mould model, which assume that a contact interface exists between the part surface and the mould wall. Before the part is ejected, the deformation of warpage has been developed inside the mould. However, the part cannot shrink and deform freely due to constraints by the rigid mould. Calculate the in-mould constraint induced part warpage to enhance the analysis accuracy.

The warpage analysis procedure is separated into two steps. The first step is mould-constraint deformation from EOP (End of Packing) to EOC (End of Cooling) which consider the effect of in-mould constraint. The second step is free deformation after the part cools to air temperature. [1,9]

4.2 Solid model in Moldex3D

The Shell-Flow model, as described for the shell model, cannot catch the 3D phenomena, such as flow area change, flow passing spheres, flow through a small dimension-to-thickness ratio area. In these cases, the simulation from the 2.5D-based CAE are less accurate or even misleading. Therefore, 3D-based CAE analysis is necessary to capture the 3D flow phenomena. The warpage analysis for the solid model follows the same procedure as for shell model. See section 4.1.3 for shell model.

4.2.1 Flow and packing analysis

The injection moulding process is basically a three-dimensional, transient problem with moving melt front. Let *x* and *y* donate the planar coordinates and *z* through the thickness direction, the velocity components *u*, *v*, *w* are in *x*, *y*, *z* direction respectively.

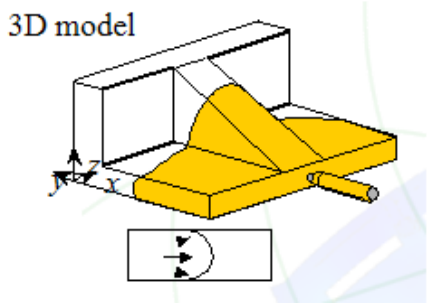

Figure 4.4 Example of a 3D model, image from [9].

Moldex3D Solid both support the assumption that the polymer melt are incompressible and compressible, in this work, the polymer melt is assumed to be compressible The governed equations for Solid-Flow model are the conservation of mass, the conservation of momentum, and the conservation of energy.

$$\text{Continuity:} \qquad \frac{\partial \rho}{\partial t} + \nabla \cdot (\rho \mathbf{u}) = 0 \tag{4.20}$$

where **u** is the velocity vector.

$$Momentum: \qquad \rho \frac{D\boldsymbol{u}}{Dt} = -\nabla p + \nabla \cdot \boldsymbol{\tau} + \rho \boldsymbol{g} \tag{4.21}$$

where p is the pressure, ρ the density, t is the time, $\boldsymbol{\tau}$ is the second-order deviatoric stress tensor and $\boldsymbol{g}$ is the body force vector

$$Energy: \qquad \rho C_p \frac{DT}{Dt} = -\nabla \cdot \mathbf{q} - \mathrm{T}\left[\frac{\partial p}{\partial T}\right]_v (\nabla \cdot \mathbf{u}) + \boldsymbol{\tau} : \nabla \mathbf{u} + \dot{S} \tag{4.22}$$

where T the temperature, C_p the specific heat, v is the specific volume, $\dot{S}$ is the rate of heat generation due to chemical reaction and **q** heat flux vector.

In a three-dimensional flow simulation, it is very important to accurately track the evolution of the melt front, which means the polymer-air interface. The melt front can be tracked by solving the transport equation, of the fractional volume function, f.

$$\frac{\partial f}{\partial t} + \nabla \cdot (\boldsymbol{u} f) = 0 \tag{4.23}$$

Here, $f = 0$ is defined as the air phase and $f = 1$ as the volume of the cavity is filled with polymer. The melt front is located within cells with $0 < f < 1$.

In order to simulate the three-dimensional mould filling flow, it is required to solve the Equations 4.20-4.22 and tracking the melt front at every time step. To solve this problem, the polymeric feature needs to be described suitably, which could be done with the viscosity model in section 3.4.2, viscoelasticity model in section 3.4.4 and the PVT model in section 3.4.6. The algorithms of the simulation can be classified into the following steps, with given initial and boundary conditions. [9,17]

1. Solving the governing equations.
2. Updating the polymer melt front.
3. Updating the material properties.
4. Repeating steps 1-3 until the entire domain is filled.

4.2.2 Cool analysis for solid model

For the solid model, both a cycle-average mould temperature approach and full transient method are supported. The cycle-average mould temperature approach is the same as for the shell model, see section 4.1.2, and will not be included in this section.

The difference between the cycle-average mould temperature approach and the full transient Method are shown in Figure 4.5. The full transient method will give a varying mould temperature during whole moulding cycle, while the cycle-average mould temperature approach will have a constant value.

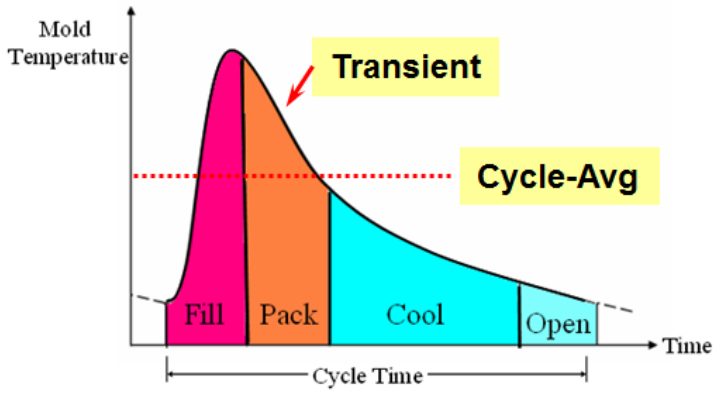

Figure 4.5 The mould temperature variation for cycle-average mould temperature approach and full transient method. [9]

The three-dimensional transient heat conduction gives the temperature field in the mould.

$$k_m\left(\frac{\partial^2 T_m}{\partial x^2}+\frac{\partial^2 T_m}{\partial y^2}+\frac{\partial^2 T_m}{\partial z^2}\right)=\rho_m C_m\frac{\partial T_m}{\partial t} \tag{4.24}$$

where T_m is the mould temperature, k_m is the mould thermal conductivity, ρ_m is the mould density and C_m is the specific heat of the mould.

The boundary of the mould, Γ, includes the cavity surface, Γ_p, the cooling channel surface, Γ_c, and the external surface, Γ_e. The boundary conditions are as follows:

- Mould cavity surface

$$k_m\frac{\partial T}{\partial n}=-q,\quad in\ \Gamma_p \tag{4.25}$$

  where q is the heat flux across the melt and mould interface.

- Cooling channel surface

$$k_m\frac{\partial T}{\partial n}=-h_f(T_w-T_c),\quad in\ \Gamma_c \tag{4.26}$$

  where h_f is the heat transfer coefficient between the mould and the coolant, T_w is the interface temperature between mould and cooling channels, and T_c is the coolant temperature. The heat transfer coefficient h_f is given in the same way as for shell; see Section 4.1.2 for more details.

- Mould exterior surface

$$k_m \frac{\partial T}{\partial n} = -h_a(T_s - T_a), \quad in\ \Gamma_e \tag{4.27}$$

where T_s is the interface temperature between mould surface and air, T_a is the temperature of the ambient air and h_a is the heat transfer coefficient between the mould and the ambient air. h_a is given in the same way as for shell; see Section 4.1.2 for more details.

The normal cooling channel analysis is applied in the same way as for shell which assumes that the rise of coolant temperature is neglected, which results in that the coolant temperature in Equation 4.26 is considered as a constant value during the cycle. [1,9]

5 Analyses

In this section, the work flow describing the procedure to simulate the injection moulding process and how the results are exported to other FEA structure analysis softwares are described. In addition, a comparison between shell and solid model is presented. Since the number of elements through the thickness is crucial for the solid model, an investigation on 3, 5 and 7 elements through the thickness are investigated. Finally, the influence of process parameters on residual stress is presented.

5.1 Moldex3D

Figure 5.1 shows the work flow to simulate the injection moulding process. The geometry is imported in HyperMold/Shell or HyperMold/Solid respectively, where the geometry is meshed, feed system and cooling channels are defined. There are two options when exporting to Moldex3D, StandardCool and FastCool respectively. The difference between these two models is how the mesh is generated for the mould and cooling channels. In this work, FastCool is used which is Moldex3D special technology and generates 3D mesh for the mould and the cooling channels automatically. In standardCool, the mesh has to be generated manually.

The HyperMold model is then imported in Moldex3D R11. The procedures to prepare the model for simulation in Moldex3D are as follows:

- Import mesh file which was created in HyperMold
- Select material from Moldex3D material database or import from file
- Specify the process conditions
- Specify the computation parameters
- Check run data

Next step is to set analysis sequence. As mentioned above, there are some different analyses available in Moldex3D:

- Flow analysis
- Packing analysis
- Cooling analysis
- Warpage analysis

The viscoelasticity calculation is only available in Moldex3D/Solid which can predict the residual stresses causes by the injection moulding process.

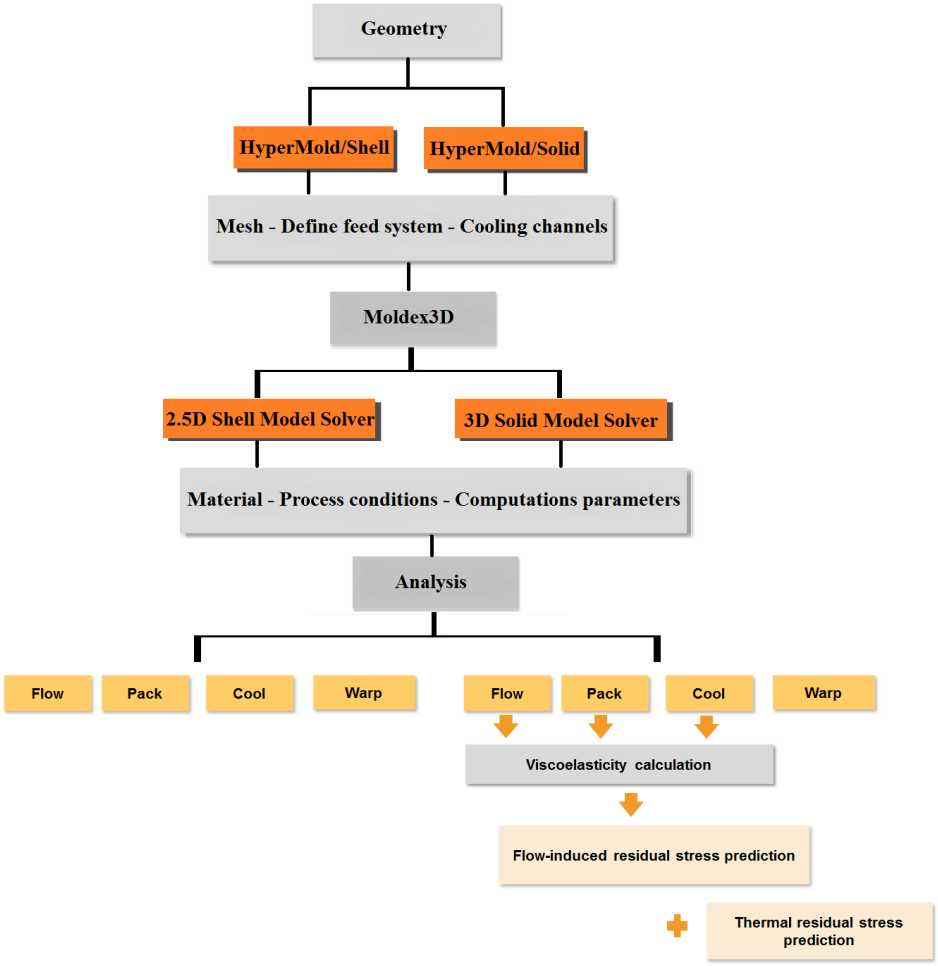

Figure 5.1 Work flow to simulate the injection moulding process in Moldex3D.

5.2 Moldex3D FEA Interface

Moldex3D FEA Interface modules provide a bridge between injection moulding CAE and other FEA structure analysis softwares. After the simulation, Moldex3D data can be translated to Abaqus, Ansys, MSC Nastran, NASTRAN, LS-Dyna, MSC Marc, NX Nastran and Radioss data. The exported data could include the original mesh, warpage mesh and material properties. The original mesh describes the geometry before moulding process, and warpage mesh describes the geometry of the moulded part. The material properties that are exported are; material stiffness, thermal expansion coefficient, density etc. When exporting solid elements the parabolic element type has to be chosen which is needed for the structural analysis.

In a parallel project, Abaqus is used to evaluate how the residual stresses affect the modal analysis. The main steps from the injection moulding simulation in Moldex3D to a modal analysis in Abaqus are shown in Figure 5.2. After the simulation of the injection moulding process, the model is exported to Abaqus as initial strain, but Abaqus does not allow initial strain condition to be stored directly, therefore, Moldex3D FEA Interface for Abaqus presents initial strain condition by the temperature difference and CLTE (Coefficient of linear thermal expansion). Combining these two properties, Abaqus will be able to calculate the deformation of the part.

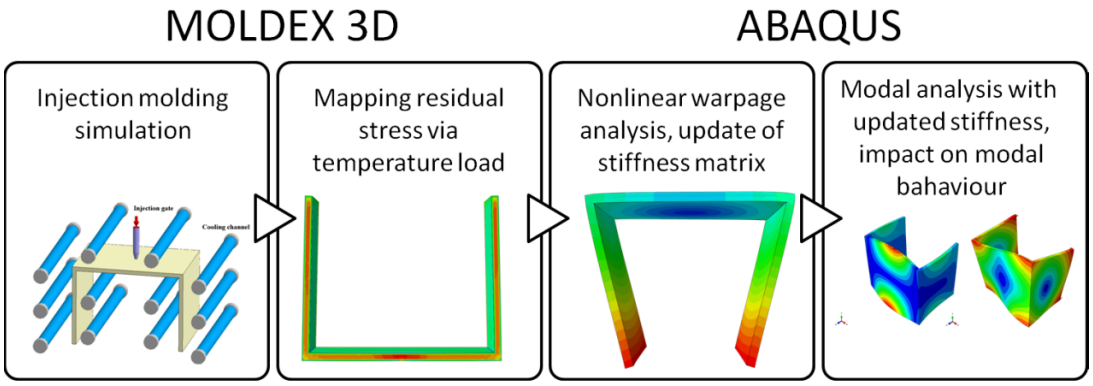

Figure 5.2 *Main steps from the injection moulding simulation to a modal analysis in Abaqus.*

5.3 Material

The polymeric material used in all injection moulding simulations in this work is Terluran GP-22. It is an easy flowing grade of ABS (Acrylonitrile Butadiene Styrene) with high resistance to impact and heat deflection, see Section 3.3 Some of the material properties for Terluran GP-22 can be seen in Table 5.1

Table 5.1 *Material properties for Terluran GP-22 [18]*

	Nominal Value Unit
Specific Gravity	1.04 g/cm^2
Melt Volume-Flow Rate (MVR)	
$200°/5.0\ kg$	1.50 $cm^2/10\ min$
$220°/10.0\ kg$	19.0 $cm^2/10\ min$
$230°/3.8\ kg$	4.80 $cm^2/10\ min$
Moulding Shrinkage – Flow	0.55 %
Water Absorption (Saturation, $23°C$)	1.0%
Tensile Modulus ($23°C$)	2300 MPa
Tensile Strength	
Yield, $23°C$	45.0 MPa
Yield, $-40°C$	63.0 MPa
Yield, $80°C$	19.0 MPa
Break ($51mm/$min)	34.0 MPa

5.4 Comparison between shell and solid model

A comparison between shell and solid modelling was performed to evaluate the difference between the two models. The evaluated structure was a u profile structure, the geometry can be seen in Figure 5.3. The reason for this profile instead of a plate is to capture the 3D phenomena in the sharp corners. In this comparison, only the mesh differs between the two models and all process and material parameters are the same.

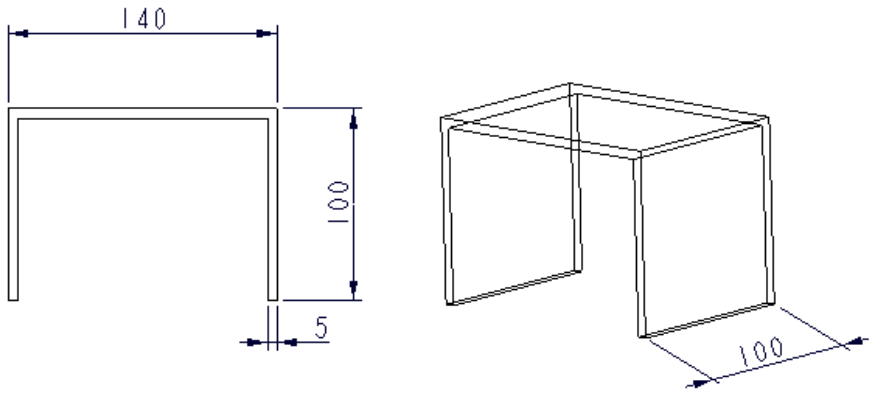

Figure 5.3 Geometry of the u profile structure in mm.

The cooling channels were defined referring to the Moldex3D guide. With a part thickness (w) of 5 mm, the cooling channel diameter (D) should be between 12 and 15 mm. In this case, the diameter of 15 mm was chosen. In order to define the distance between channel centers (C) and distance between channel and part (H), the following rule of thumb can be used:

$$C = 3 \times D = 45\ mm$$

$$H = 2 \times D = 30\ mm$$

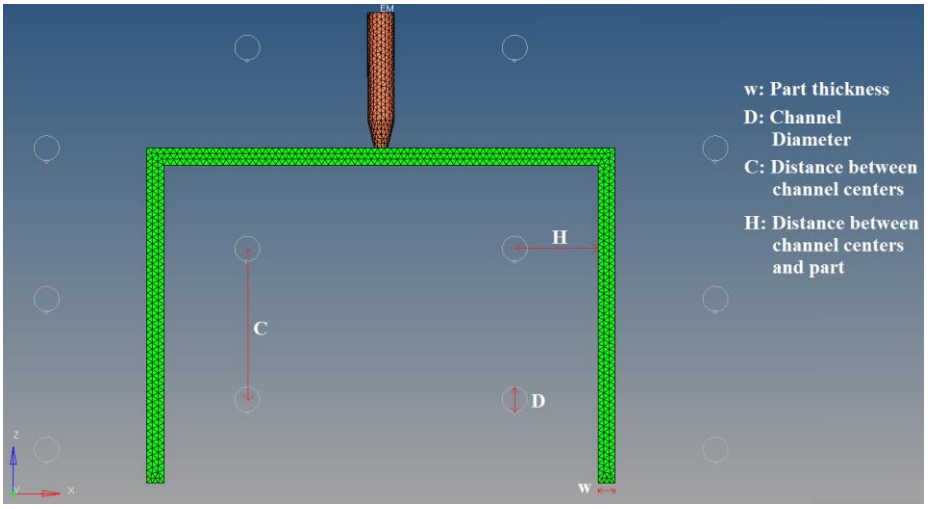

Figure 5.4 Location and definition of cooling channels.

For the shell model, HyperMold/Shell was used as pre-processor to create a midsurface with assigned thickness. The midsurface was meshed, cooling channel and melt entrance were defined. The model can be seen in Figure 5.5.

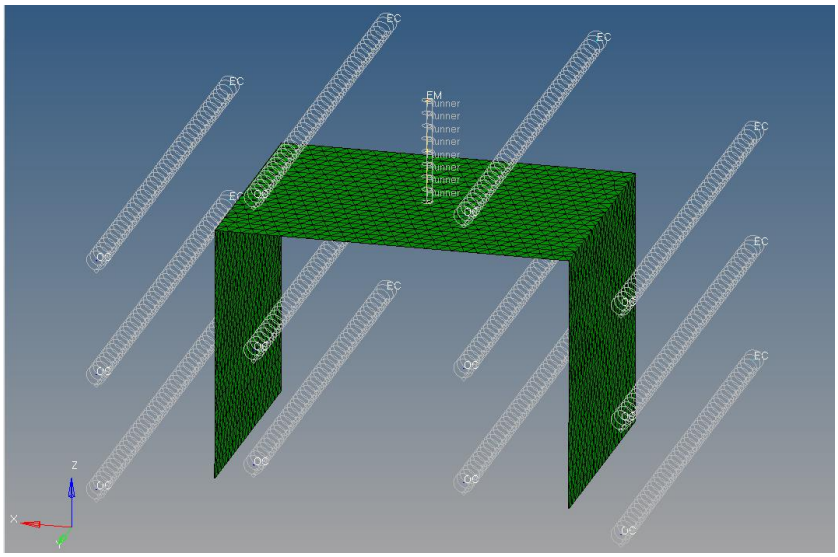

Figure 5.5 HyperMold/Shell is used as pre-processor.

HyperMold/Solid was used as pre-processor for the solid model. Where the model was meshed and the melt entrance and cooling channels were defined at the same location as for the shell model. The model can be seen in Figure 5.6.

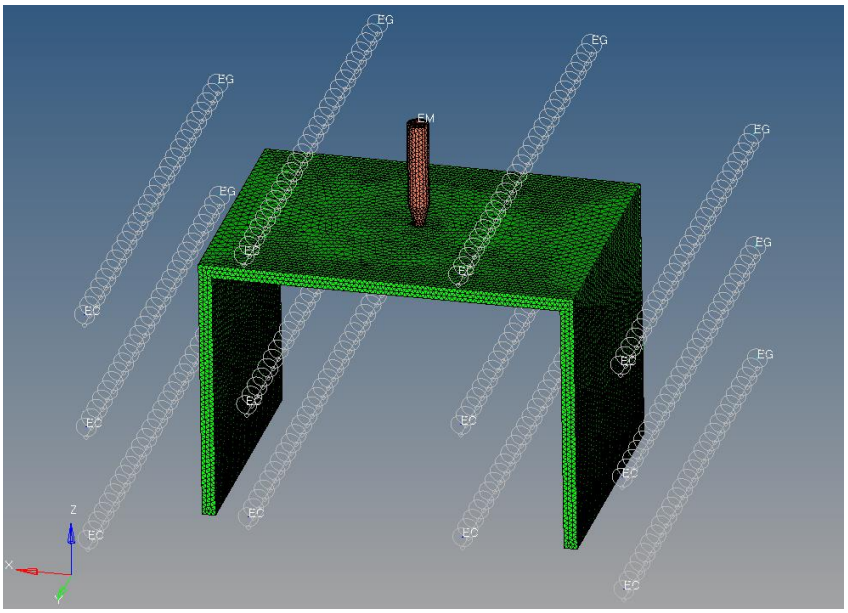

Figure 5.6 HyperMold/Solid used as pre-processor.

The injection moulding simulation was performed in Moldex3D. The material and process parameters can be seen in Table 5.2 below, and will be referred as the standard table in this work. The injection pressure profile is defined as 70% of the maximum injection pressure during the filling process. The switchover point from filling to packing stage occurs when 98% of the cavity volume is filled. The specified packing time after the filling simulation is set to 5 seconds and the maximum packing pressure is used during the whole packing stage. The mould temperature is 50 °C at the beginning of the simulation and applies as initial condition. Moldex3D assumes that the boundary temperature is uniform, but in this case, a cooling analysis has been done before the filling and packing simulation to estimate the average mould temperature distribution during the cycle, which is used in the filling and packing

simulation. The temperature of the polymer melt is set to 250 °C at the inlet on top of the runner.

Table 5.2 Process parameters and material for the comparison between shell and solid model.

Material	TerluranGP-22 from
Maximum injection pressure	164 MPa
Maximum packing pressure	164 MPa
Maximum clamping force	1373 kN
Packing time	8 sec
Melt temperature	250 °C
Mould temperature	50 °C
Air temperature	25 °C
Eject temperature	110 °C
Cooling time	40 sec
Mould-open time	5 sec
Cooling channels • Coolant temperature • Coolant flow rate • Coolant • Diameter	 50 °C 120 cm^3/sec water 15 mm
Mould material: • Density • Heat Capacity • Thermal conductivity • Elastic modulus • Poisson ratio • CLTE	 8 g/cm^3 $5 \cdot 10^6$ $erg/(g.K)$ $5 \cdot 10^6$ $erg/(sec.cm.K)$ $2 \cdot 10^{12}$ $dyne/cm^2$ 0.3 0.00012 $1/K$

In this comparison, the cycle-average mould temperature approach is used in both shell and solid model, because the full transient method is not supported for shell model. The analysis sequence is set to C F P C W (Cooling, Filling, Packing, Cooling, Warpage). In the warpage analysis for the solid model, the element type is set to parabolic.

To easily compare the results from shell and solid models, measure nodes (MN) are defined according to Figure 5.7. The Viscoelasticity model is not supported for the shell model and, consequently, no residual stress results can be obtained. The warpage results from the two models will be compared since warpage is a direct result from residual stress.

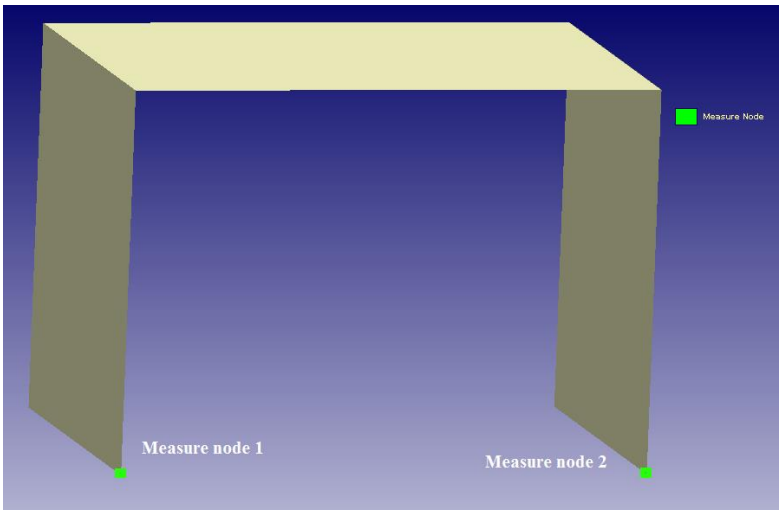

Figure 5.7 *Shows the location of the measure nodes (MN) that are used to compare the different models.*

In Table 5.3, the results from the warpage analysis from both shell and solid model are shown. The x-directions is along the measure nodes 1 and 2, the coordinate system can be seen in Figure 5.6. Clearly, the number of integration points (points through the thickness) for the shell model does not affect the results. Therefore, only 15 integrations points were considered in the finer mesh. The 3, 5 and 7 elements through the thickness give 7, 11 and 15 nodes through the thickness, since quadratic elements are used.

Table 5.3 *Results from warpage analysis for shell and solid model, all values are in mm.*

		Shell						**Solid**		
		Number of integration points						Number of elements through the thickness		
		Number of elements: 16392			Number of elements: 21025					
	MN	6	15	30	6	15	30	3	5	7
x-Displacement	1	-2.949	-2.911	-2.911	---	-2.873	---	-3.772	-3.345	-3.184
	2	2.941	2.903	2.902	---	2.904	---	3.785	3.216	3.207
Total-Displacement	1	3.581	3.556	3.555	---	3.523	---	3.998	3.594	3.434
	2	3.573	3.546	3.545	---	3.550	---	4.005	3.466	3.556

According to Table 5.3, the x-displacement for the shell model is lower than for the solid model, but the total displacement is almost the same in both models for 5 and 7 elements through the thickness. For 5 elements through the thickness, the total displacement in measure node 1 is 3.594 mm while it is 3.556 mm for the shell model with 15 integration points.

For this geometry, the shell model captures the warpage phenomena properly in Moldex3D, but when the shell model is exported with Moldex3D FEA Interface to Abaqus, the temperature difference through the thickness is not included which results in unrealistic warpage. This problem was reported to Moldex3D support. Since this problem could not be solved, the focus in the subsequent analysis was on solid elements. The results from warpage analysis with the solid model in Abaqus for 5 elements through the thickness can be seen below in Figure 5.8.

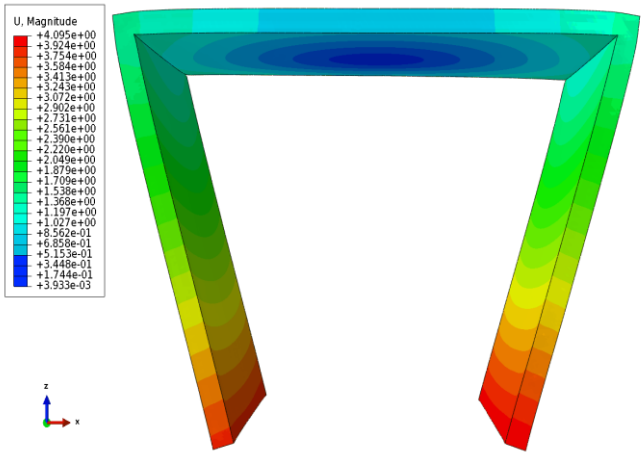

Figure 5.8 *Warpage result in Abaqus with 5 elements through the thickness.*

The warpage results from both Moldex3D/Solid and Abaqus, where the total displacement in measure node 2 are compared, can be seen in Table 5.4.

Table 5.4 *Total warpage results from Moldex3D/Solid and Abaqus, values are in mm.*

	Moldex3D/Solid [mm]	**Abaqus [mm]**
3 elements through the thickness	4.005	4.511
5 elements through the thickness	3.466	4.095
7 elements through the thickness	3.556	3.908

As shown in Table 5.4, the warpage results from Abaqus is approximately 13% higher than Moldex3D/Solid, although the same mesh and element type are used in both calculations. The reason for the difference is unknown.

The advantage of using shell model is that it takes significantly less computation time, approximately 15 minutes. For the solid model it takes approximately 3 hours. However, since the Moldex3D FEA Interface to Abaqus does not work for shell elements, the solid model will be used in order to easily determine how the process parameters influence the residual stress.

5.5 Element layers for solid model

In next section, the influence of process parameters on residual stresses is investigated. The number of elements through the part thickness is important for injection moulding CAE analysis. For example, the temperature distribution across the part thickness can be seen in Figure 5.9. The temperature rises sharply close to the cavity walls and decreases down slowly until the middle of the part. The element resolution is the key point to obtain the distribution through the thickness.

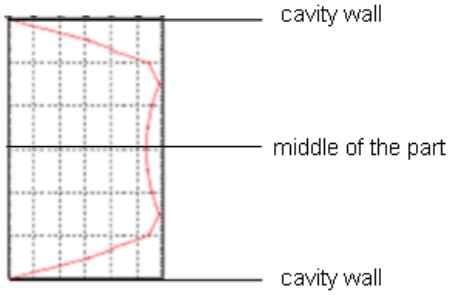

Figure 5.9 Temperature distribution across the part thickness.

In this section, 3, 5 and 7 elements through the thickness are investigated. The same geometry, material, process conditions and computation parameters was used as in section 5.4 for solid model, see also Table 5.2.

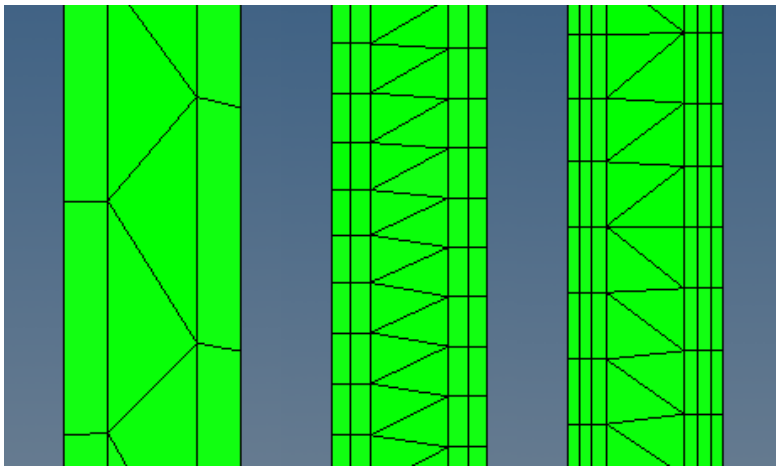

Figure 5.10 Shows the mesh for 3, 5 and 7 elements through the thickness.

The different meshes can be seen in Figure 5.10. According to Figure 5.9, the most happens close to the cavity walls and in order to capture the frozen layer, there are thinner elements close to cavity walls.

The thermal-induced residual stress from Moldex3D in z-direction (σ_{zz}) can be seen in Figure 5.11 for 3, 5 and 7 elements through the thickness respectively. Were the

thermal-induced residual stresses are taken from after warpage and in the cross section as shown in Figure 5.12.

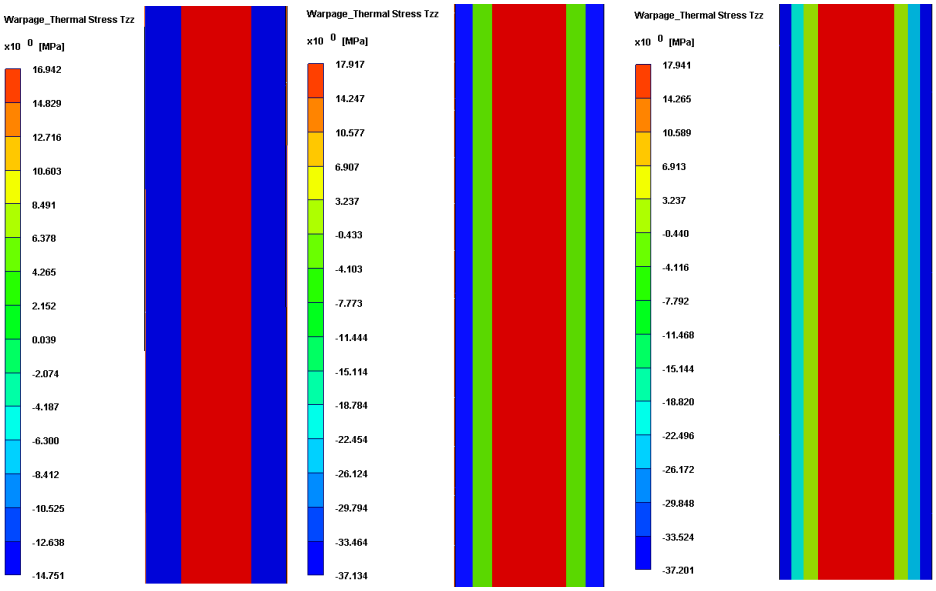

Figure 5.11 Thermal-induced residual stress in z-direction (σ_{zz}) for 3, 5 and 7 elements through the thickness respectively in Moldex3D.

Figure 5.11 shows that it is a quite large difference between 3 and 5 elements through the thickness, from approximately -15 MPa in the outer layers for 3 elements through the thickness to -37 MPa and -7 MPa (green area) respectively in the two outer layers for 5 elements through the thickness. But the highest compression and tensile stresses for 5 and 7 elements through the thickness are almost the same in Moldex3D. To compare the residual stresses from Moldex3D with Abaqus, the residual stresses from Abaqus is shown in Figure 5.12, there is a large difference between the highest compression stresses for 3 elements through the thickness. In Moldex3D the highest compression stress in σ_{zz} is approximately 15 MPa compared to 40 MPa (S33) in Abaqus for 3 elements through the thickness, while both results in the same highest tensile stress of 17 MPa. The same appearance is shown for 5 and 7 elements through the thickness, but the highest compression stresses are closer to each other, in Abaqus the highest compression stress is approximately 43 MPa while it is 37 MPa in Moldex3D for 5 and 7 elements through the thickness. The highest tensile stress is almost the same for both Moldex3D and Abaqus for 5 and 7 elements through the thickness. Since the results from 5 and 7 layers do not differ so much and due to the long computation time for more elements through the thickness, 7 layers will be enough in this work and are used in further investigation. 7 layers will capture the distribution through the thickness better than 5 elements through the thickness.

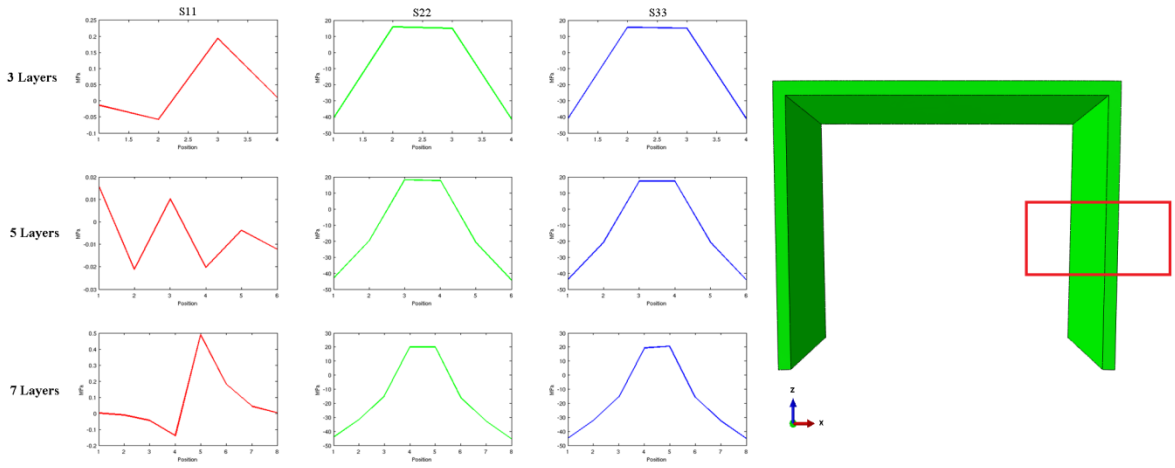

Figure 5.12 Residual stress comparisons for the various numbers of elements through the thickness in Abaqus.

For larger models, number of elements increases dramatically with increased number of element through the thickness. When trying to decrease the total element number but still having the same number of elements through the thickness, often results in bad elements, because one side of the element increases while the height is the same due to part thickness. The bad elements made it impossible for the solver to calculate the polymeric flow and result in incomplete filling.

5.6 Influence of process parameters on residual stress

The process parameters are crucial for the appearance and properties of the final product. In order to determine how the process parameters influence the residual stresses, only one parameter is changed at the time.

The same u profile structure was used as in Section 5.4, the solid model. The process parameters in Table 5.2 are used and the deviations from the table are mention in each section below.

In this investigation the full transient method for cooling analysis is used. The analysis sequence is set to Ct F P Ct W (Cooling transient, Filling, Packing, Cooling transient, Warpage). The viscoelasticity model is used, in order to predict the residual stresses.

In following sections, the result will be taken from the same location on the u-profile, Figure 5.13 shows the location of the measure node and the cross section. The warpage results and the flow-induced residual stresses are compared in the measure node, thermal induced residual stresses are taken from the cross section. To clarify, the residual stresses in the following sections are the stresses remaining after warpage.

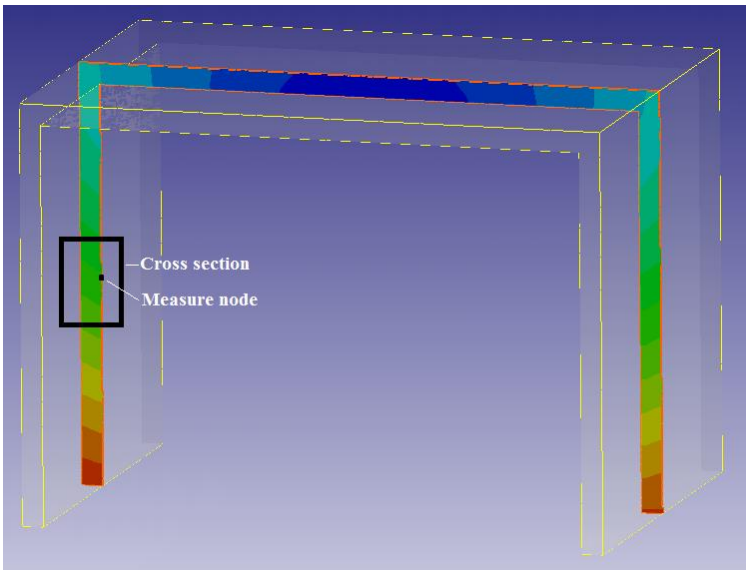

Figure 5.13 Location of measure node and cross section.

5.6.1 Effect of Cooling

To investigate the effect of cooling, the coolant temperature is varied in each simulation. The coolant temperatures used are 90 $C°$, 70 $C°$, 50 $C°$, and 30 $C°$ respectively. A coolant temperature of 10 $C°$ was also considered, but the high cooling rate resulted in that the gate froze and that the cavity was not filled completely.

The warpage results are shown in Figure 5.14, where the total displacement in the measure node for the various coolant temperatures is shown. Clearly, the total displacement increases with higher coolant temperature.

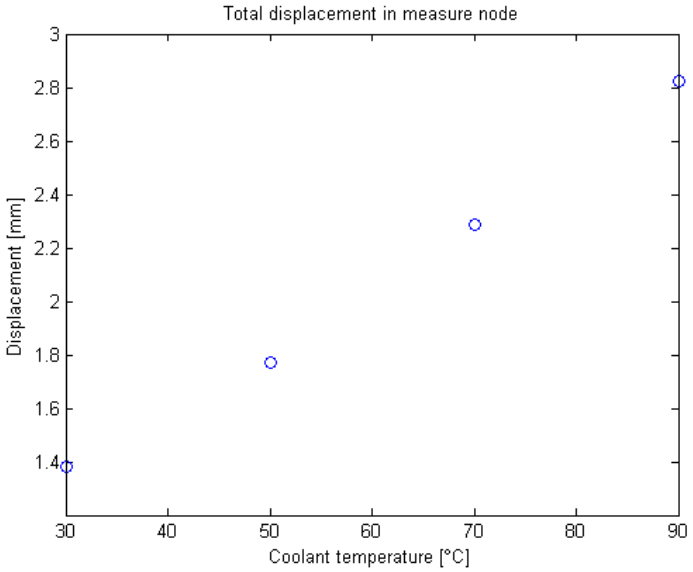

Figure 5.14 Total displacement in measure node for the different coolant temperatures.

The flow-induced residual stress effect on the displacement is shown in Figure 5.15 for the various coolant temperatures. The slightly increase of the flow-induced residual stress effect on displacement with higher coolant temperature is probably due

to the increase of shear rate during filling. The shear rate in EOF (End of filling) for the coolant temperatures of 30 $C°$, 50 $C°$, 70 $C°$ and 90 $C°$ are 0.2462, 0.3561, 0.4921 and 0.7689 $1/s$ respectively. The increase of shear rate results in that the polymer chains are sheared and elongated in a higher extent, which results in higher flow-induced residual stress.

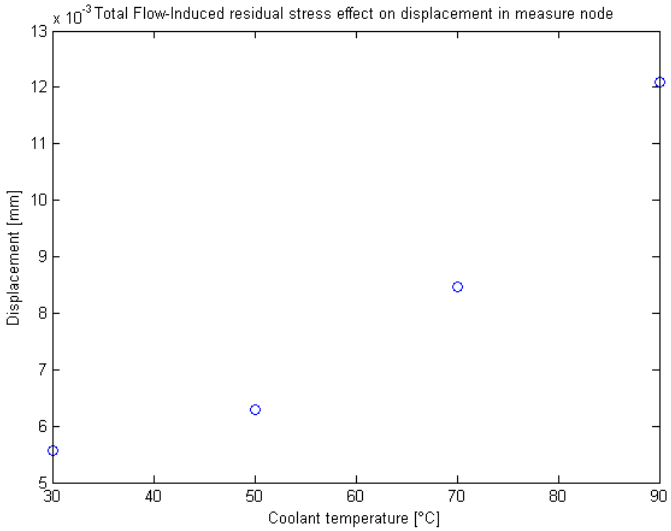

Figure 5.15 *Total flow-induced residual stress effect on displacement for different coolant temperatures.*

The thermally-induced residual stresses for the coolant temperature of 90 $C°$ are shown in Figure 5.16. The appearance of the stress distribution is the same for all coolant temperatures, thus the σ_{yy} and σ_{zz} have the highest tensile stresses in the core and highest compression stresses closest to the cavity walls.

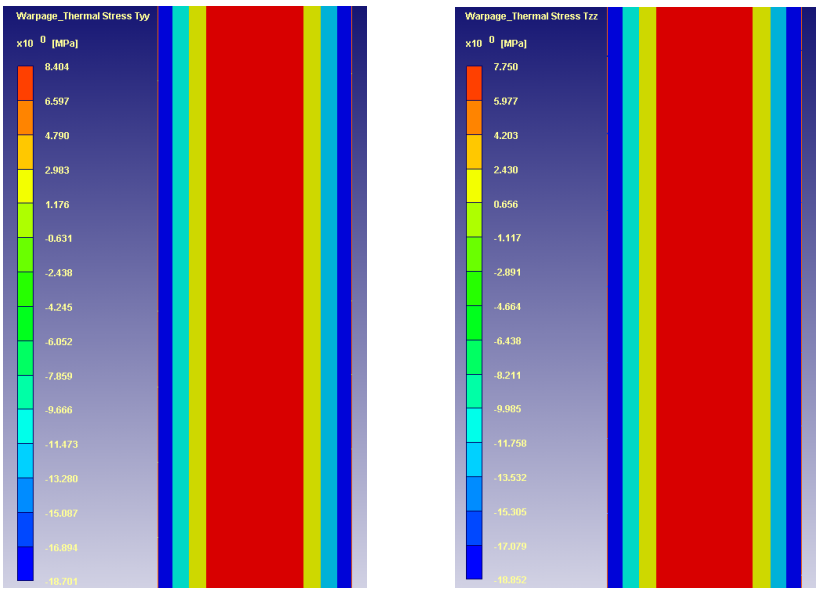

(a) (b)

Figure 5.16 *The thermally-induced residual stress for the coolant temperature of 90 C°, (a) σ_{yy} and (b) σ_{zz}.*

The variation of the thermally-induced residual stresses for the different coolant temperatures can be seen in Figure 5.17. The thermal-induced residual stresses shown in the figure are the maximum tensile stress in the cross section *i.e.* in the core. According to the results, the thermally induced residual stresses decrease with higher coolant temperature. One explanation for this is differential shrinkage. A lower coolant temperature will result in lower temperature at the cavity walls, thereby a higher temperature difference between the core and cavity walls.

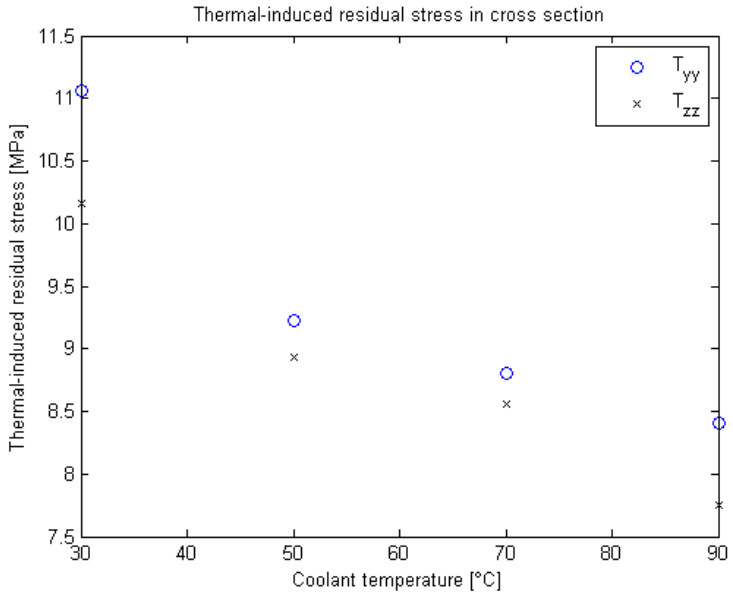

Figure 5.17 Thermal-induced residual stress for different coolant temperatures.

5.6.2 Effect of melt temperature

The suggested melt temperature for Terluran GP-22 should be between 220 $C°$ and 280 $C°$. In this investigation, the melt temperatures are set to 220, 240, 250, 260 and 280 $C°$ respectively. The other process parameters used can be seen in Table 5.2.

The warpage results for the different melt temperatures are shown in Figure 5.18, where the total displacement in measure node in Figure 5.13 are used. Clearly, the total displacement increases with higher melt temperature.

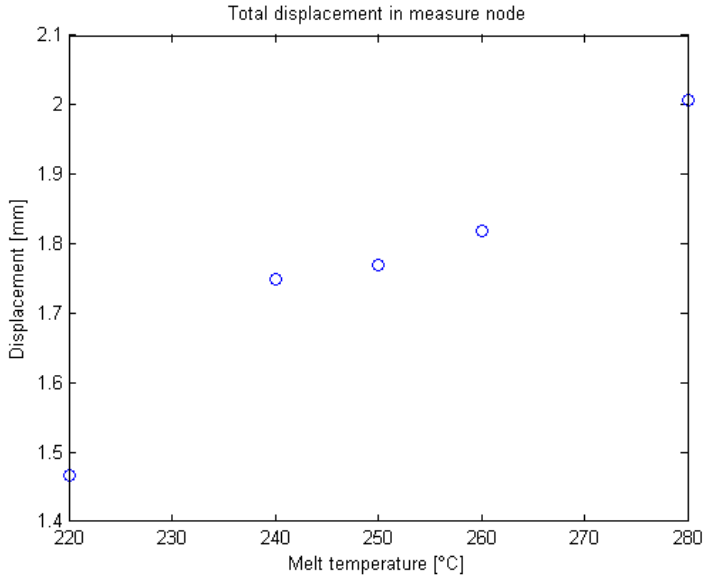

Figure 5.18 Total displacement in measure node for various melt temperatures.

The flow-induced residual stress effect on displacement is shown in Figure 5.19 for the various melt temperatures. For the temperatures above 240 $C°$, the flow-induced residual stress effect on displacement are almost constant, but for 220 $C°$, there is a high effect on displacement.

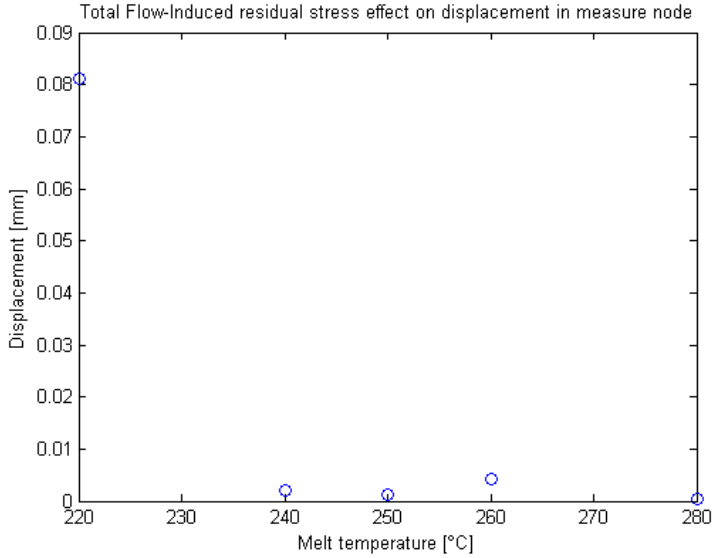

Figure 5.19 Total flow-induced residual stress effect on displacement for various melt temperatures.

The thermally-induced residual stresses for the melt temperature of 220 $C°$ are shown in Figure 5.20. The appearance of the stress distribution is the same for all melt temperatures, thus the σ_{yy} and σ_{zz} have the highest tensile stresses in the core and highest compression stress closest to the cavity walls.

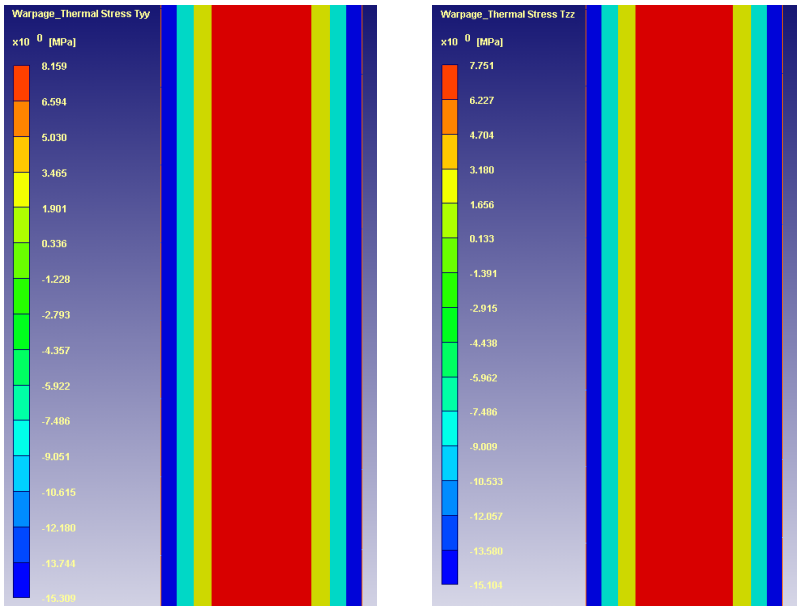

(a) (b)

Figure 5.20 *Thermally-induced residual stress for melt temperatures of 220, (a) σ_{yy} and (b) σ_{zz}.*

The variation of the maximum thermally-induced residual stress for the different melt temperatures are shown in Figure 5.21. According to the results, the thermally induced residual stresses increases with higher melt temperature. This may due to that polymer shrink in a higher degree for higher temperatures, and a higher melt temperature will increase the temperature difference between core and cavity walls, which may results in higher residual stresses.

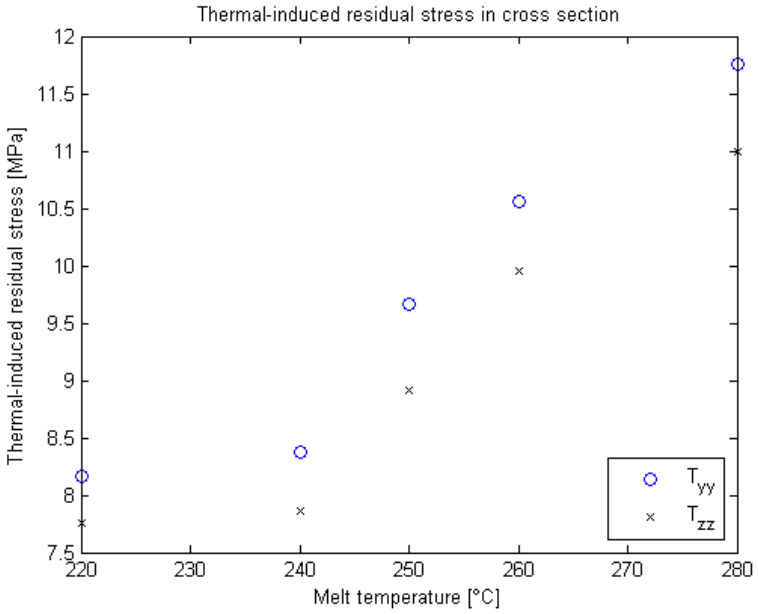

Figure 5.21 *Thermal-induced residual stress for various melt temperatures.*

5.6.3 Effect of packing pressure

To investigate the effect of packing pressure, the pressure is changed in each simulation. The same process parameters are used as in Table 5.2, and the different packing pressures used are 10 MPa, 20MPa, 30MPa, 40MPa and 50MPa respectively.

The warpage in the measure node is shown in Figure 5.22 for the different packing pressures. The total displacement does not indicate a specific behaviour for the different packing pressures and are almost constant.

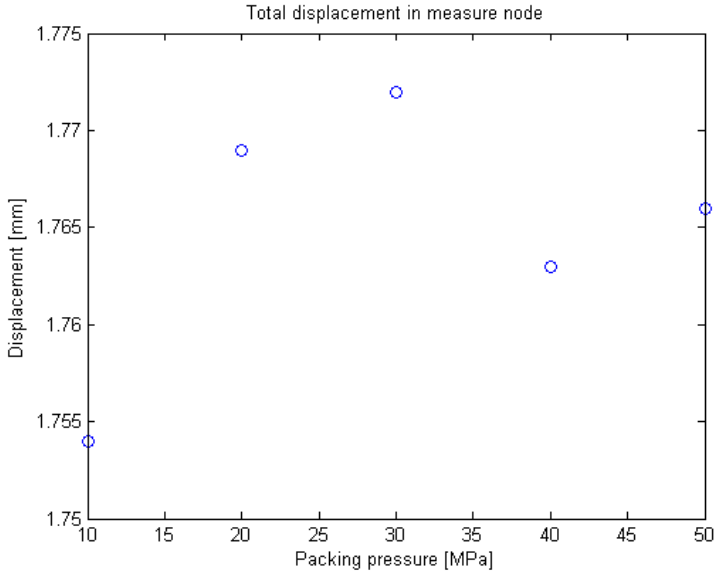

Figure 5.22 Total displacement for the different packing pressures.

The total flow-induced residual stress effect on displacement are shown in Figure 5.23 for the various packing pressures. As for the total displacement, the different packing pressures do not indicate on a specific behaviour.

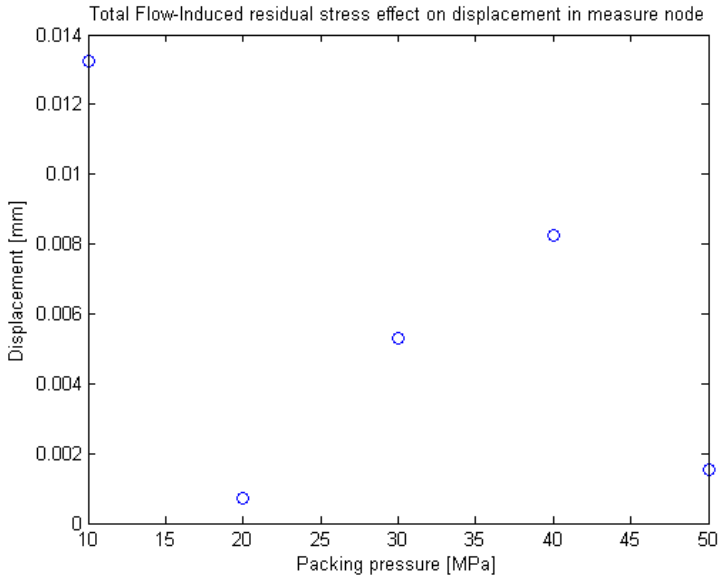

Figure 5.23 Total flow-induced residual stress effect on displacement.

The thermally-induced residual stresses for the packing pressure of 10MPa are shown in Figure 5.24. As for the other process parameters, the appearance of the stress distribution is the same for all packing pressures.

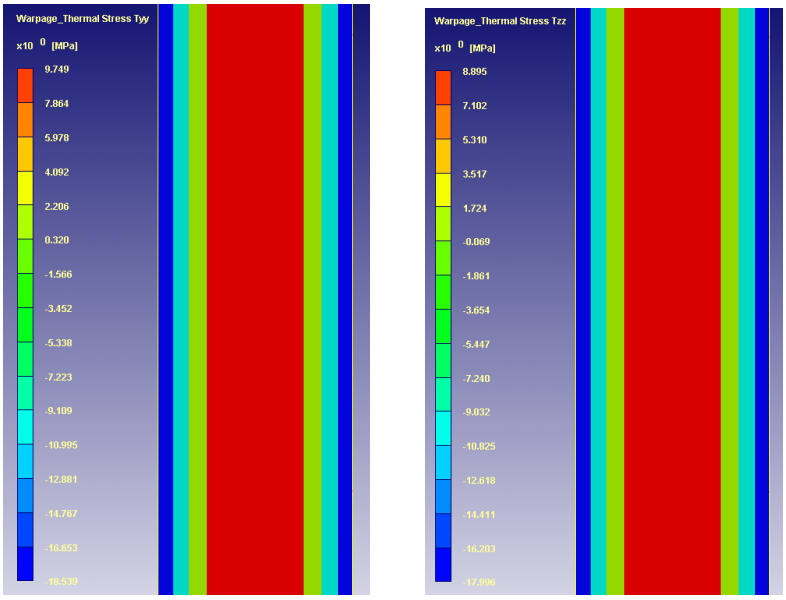

(a) (b)

Figure 5.24 Thermally-induced residual stress for a packing pressure of 10 MPa, (a) σ_{yy} and (b) σ_{zz}.

The variation of the thermally-induced residual stress for the different packing pressures is shown in Figure 5.25. According to the results, the thermally induced residual stresses in z-direction (σ_{zz}) increase with increasing packing pressure. While the thermally-induced residual stress in y-direction (σ_{yy}) starts to decrease until a packing pressure of 30 MPa and increases for a packing pressure over 30 MPa.

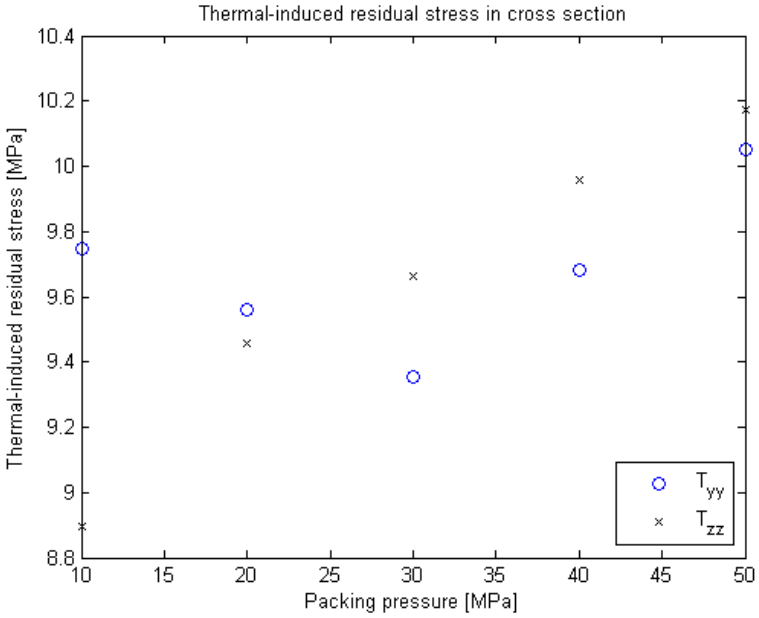

Figure 5.25 Highest thermal-induced residual stress in the cross section for the various packing pressures.

5.6.4 Effect of flow rate

The effect of flow rate was investigated, where the flow rate was changed to 20, 35, 50 and 80 m^3/s respectively. The flow rate is inversely proportional to filling time, the various flow rates with the corresponding filling time is shown in Figure 5.26.

Figure 5.26 The different flow rate will give different filling time.

The warpage results are shown in Figure 5.27, where the total displacements versus the different flow rates are shown. The total displacement increases with increasing flow rate.

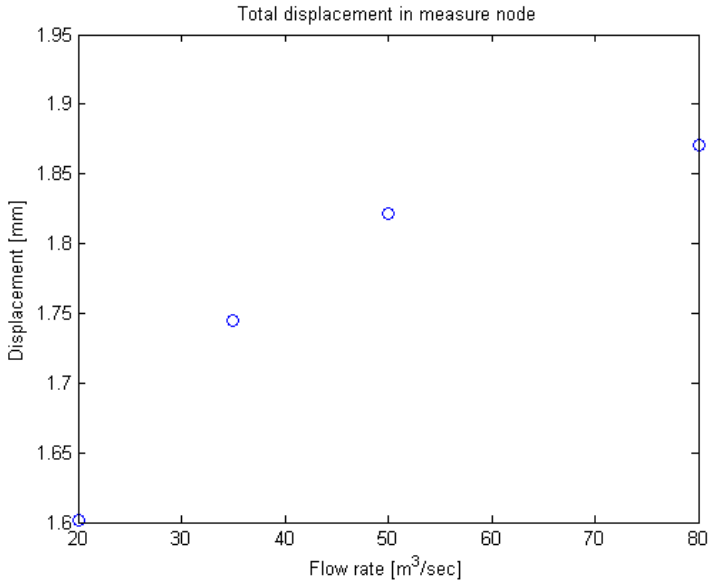

Figure 5.27 Total displacement in measure node versus the different flow rates.

The total flow-induced residual stress effect on displacement is shown in Figure 5.28 for the different flow rates. According to the results, the total flow-induced residual stress effect on displacement increase with higher flow rate.

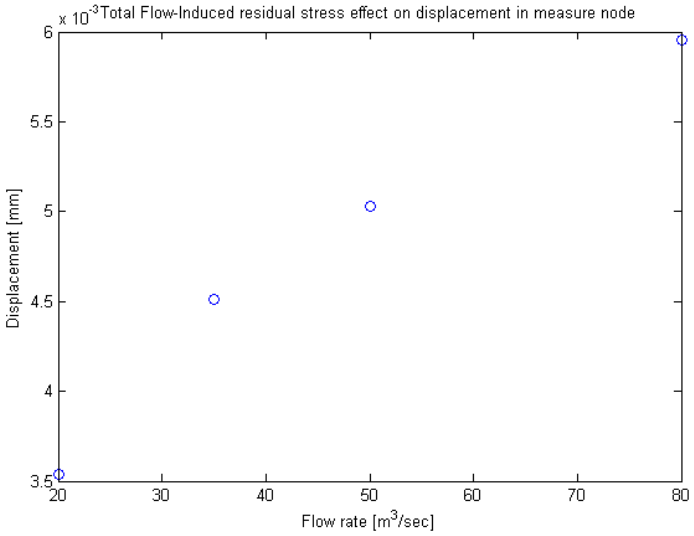

Figure 5.28 Total flow-induced residual stress effect on displacement.

The thermal-induced residual stresses with the flow rate of 20 m^3/s are shown in Figure 5.29. As for the other process parameters, the appearance of the stress distribution is the same for the various flow rates.

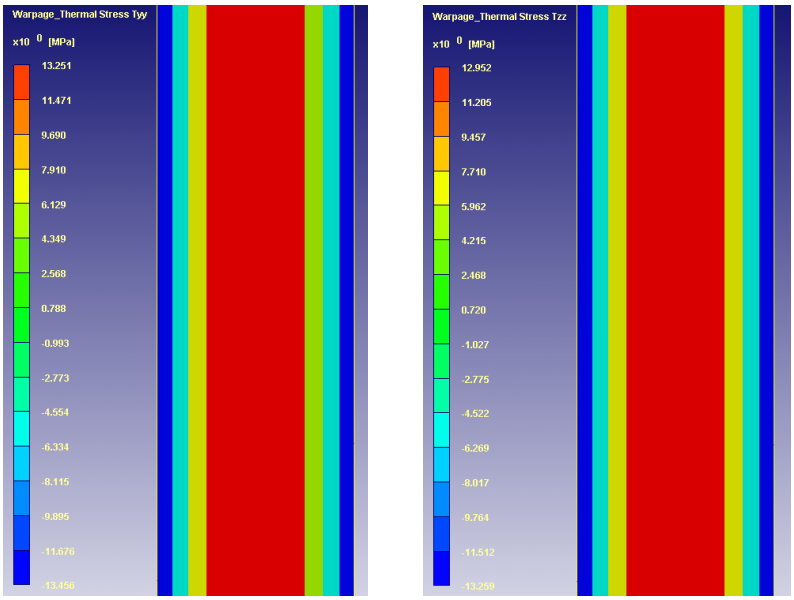

(a) (b)

Figure 5.29 The thermal-induced residual stress with the flow rate of 20, (a) σ_{yy} and (b) σ_{zz}.

The variation of the thermally-induced residual stresses for the different flow rate is shown in Figure 5.30. According to the results, the thermally induced residual stresses decrease with higher flow rate.

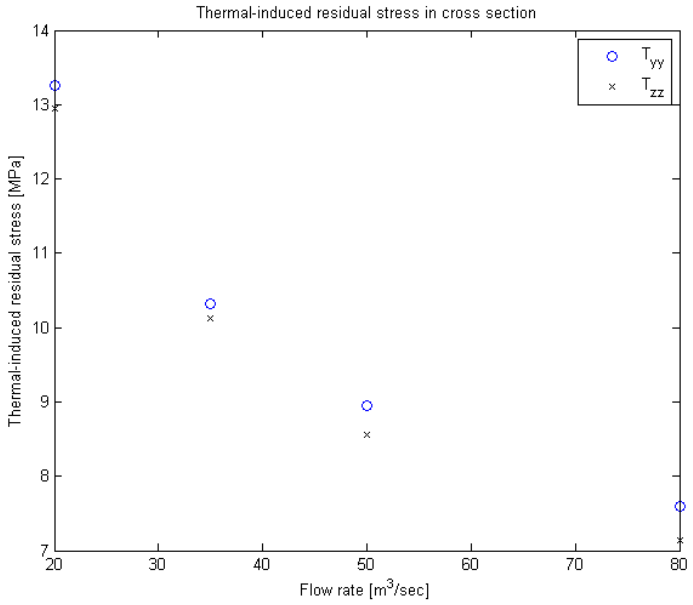

Figure 5.30 Maximum thermal induced residual stress for various flow rates.

6 Conclusion

The comparison between shell and solid modelling showed that Moldex3D can calculate the warpage results properly for the shell model. But when exporting the shell model results to Abaqus with Moldex3D FEA Interface, the temperature distribution through the thickness is not included, which results in unrealistic warpage results. In addition, Moldex3D/Shell cannot predict the residual stresses and thus there are no residual stresses to export. According to Moldex3D, Moldex3D/Shell will be extended and the modules in Moldex3D/Solid will also be supported in Moldex3D/Shell.

The warpage results in Abaqus with the solid model are approximately 13 % higher than in Moldex3D/Solid, although the same mesh and element type are used in both calculations. The reason for the difference is unknown.

In order to capture the residual stress distribution through the thickness, the number of elements through the thickness is crucial. The results show that 3 elements through the thickness do not catch the residual stress distribution suitable in Moldex3D. Furthermore, the highest compression stress is not consistent with Abaqus. 5 and 7 elements through the thickness give a better distribution and the residual stresses from Moldex3D and Abaqus corresponds better. In this work, 7 elements were assumed to be enough. But depending on the application, it may be wise to use fewer or more elements. For larger models, the number of elements increases dramatically with increased number of element through the thickness, resulting in long computation time. When trying to decrease the total element number but still having the same number of elements through the thickness, often results in bad elements due to part thickness, since one side of the element increase while the height is the same. The bad elements could result in hard to solve the polymeric flow and result in incomplete filling.

The total displacement and the flow-induced residual stress effect on displacement increases with higher coolant temperature. While the thermal-induced residual stress decreases with higher coolant temperature.

The total displacement increases with higher melt temperature. For a melt temperature over 240, the flow-induced residual stress effect on displacement is almost constant. The thermal-induced residual stresses increases with higher melt temperature.

The packing pressure does not indicate on a specific behaviour for the total displacement and the flow-induced residual stress effect on displacement. But the thermal-induced residual stress in z-direction increases with higher packing pressure, and in y-direction the stress decreases until a packing pressure of 30 MPa, over 30 MPa the stresses increases.

The total displacement and the flow-induced residual stress effect on displacement increases with higher flow rate. While the thermal-induced residual stress decreases with higher flow rate.

Generally, for all investigated process parameters, the flow-induced residual stresses are smaller than the thermal-induced residual stress. The flow-induced residual stress

effect on displacement is in order of 10^{-3} mm and does not affect the total displacement. However, for other materials and geometries, especially thin-walled geometry, it may have larger influence. In thin-wall geometries, the part is cooled and frozen in shorter time and thus the molecular orientations are not completely relaxed, resulting in frozen-in orientation which affects the mechanical anisotropy and thermal properties.

The appearance of the stress distribution is the same for all process parameters, thus the σ_{yy} and σ_{zz} have the highest tensile stresses in the core and highest compression stresses closest to the cavity walls.

7 Recommendations and future work

In the beginning of this work, Moldex3D-Designer was used as pre-processor. Moldex3D-Designer does not support shell model and the solid mesh could only be controlled by a scale from 1 to 5, where 1 is coarse mesh and 5 is the finest mesh. The element number through the thickness could not be controlled properly. Moldex3D-Designer is a great tool to quickly simulate the injection moulding process and check the design of the product, but not to use in order to predict the residual stresses.

The warpage results in Abaqus with the solid model are approximately 13 % higher than in Moldex3D/Solid, although the same mesh and element type are used in both calculations. The reason for the difference is unknown. It would be useful to find out the difference between the warpage calculation in Moldex3D and Abaqus.

To validate the simulation, the method that has been used in this work could be used on the parts supplied by Volvo Group Trucks Technology (GTT): two interior plastic parts (front and shelf). In order to run a modal analysis in Abaqus to be compared with physical tests performed at Volvo GTT.

To further increase the knowledge about how the process parameters affect the residual stress, a more detailed study could be made and compared with physical tests.

8 References

[1] R Zheng, R I.Tanner, Xi-Jun Fan (2011): Injection Molding: Integration of Theory and Modeling Methods. Springer

[2] A Azwan Bin Abdol Zahar (2009): Effects of injection molding gate mechanism on parameters machining and defects of book tray. University Malaysia

[3] Screw injection molding machine. http://www.thermosole.com (2013-01-28)

[4] A J Peacock.; A Calhoun (2006): Polymer Chemistry – Properties and Applications. Hanser Publisher

[5] Introduction to polymer. http://www.cmse.ed.ac.uk/MSE3/Topics/MSE3-polymer.pdf (2013-01-28)

[6] W D. Callister, Jr (1999) Material science and engineering; an introduction, fifth edition. John Wiley & Sons, New York

[7] M Chande, S K. Roy (2009): Industrial Polymers, Specialty Polymers, and Their Applications. CRC Press Inc

[8] Encyclopaedia -Acrylonitrile butadiene styrene. http://www.nationmaster.com/encyclopedia/Acrylonitrile-butadiene-styrene (2013-01-28)

[9] Moldex3D Help

[10] B Abbes; R Ayad; J-C Prudhomme; J-P Onteniente (1998): Numerical Simulation of Thermoplastic Wheat Starch Injection Molding Process. Polymer Engineering and Science, Vol. 39, No. 1, 2029

[11] Residual stress. http://www.dc.engr.scu.edu/cmdoc/dg_doc/develop/process/physics/b3400001.htm (2013-01-28)

[12] K-H Han, Y-T Im (1997): Compressible flow analysis of filling and post-filling in injection molding with phase-change effect. Composite Structures, Vol. 38, No. 1-4, pp. 179-190.

[13] F Bernal, M Kindelan (2007): RBF meshless modelling of non-Newtonian Hele-Shaw flow. Engineering Analysis with Boundary Elements, Vol. 31, No. 10, pp. 863-874.

[14] F W Dittus, L. M. K. Boelter: Univ. Calf. (Barkeley) Pub. Eng., Vol. 2, pp. 443, 1930

[15] JP Holman (1976): Heat transfer, 4th edition. McGraw-Hill, New York.

[16] F Ilinca, J F Hétu (2000) SPE ANTEC Papers 727

[17] S-W Kim, L-S Turng (2004): Developments of three-dimensional computer-aided engineering simulation for injection moulding. Modelling and Simulation in Materials Science and Engineering, Vol. 12, No. 3, pp. S151-S173.

[18] Data sheet. Prospector. Terluran GP-22